ACTIVE CLEANING TECHNIQUE DEVICE

DESIGN STUDY SUMMARY REPORT

D180-15454-1
MARCH 1973

CONTRACT NAS8-28270

PREPARED FOR

GEORGE C. MARSHALL ● SPACE FLIGHT CENTER
MARSHALL SPACE FLIGHT CENTER,
ALABAMA 35812

By

BOEING AEROSPACE COMPANY
RESEARCH & ENGINEERING DIVISION
SEATTLE, WASHINGTON 98124
A DIVISION OF THE BOEING COMPANY

●

ACTIVE CLEANING TECHNIQUE DEVICE

Design Study Summary Report

D180-15454-1

March 1973

by

R. L. Shannon

R. B. Gillette

Prepared Under Contract Number NAS8-28270 By

Boeing Aerospace Company

Research and Engineering Division

Seattle, Washington 98124

A Division of The Boeing Company

for

George C. Marshall Space Flight Center

Marshall Space Flight Center, Alabama 35812

ACKNOWLEDGEMENTS

The authors are grateful to the following persons for their assistance in accomplishing this study:

Mr. Heinz Recker	- Preparation of mechanical design detailed engineering drawings.
Mr. Anthony Decouteau	- Preparation of electronics design.
Mr. Freeman Laxon	- Assistance in conducting prototype tests and consultation on design problems.
Mr. Czeslaw Deminet	- Design and fabrication of quartz plasma generation tubes.
Mr. Gregory Cruz	- Assistance in development of catalytic probe.

TABLE OF CONTENTS

1.0 SUMMARY

This report describes the work accomplished under the design phase of NASA Contract NAS8-28270. The objective of this program was to develop a laboratory demonstration model (LDM) of an active cleaning technique (ACT) device. The principle of this device is based primarily on the technique for removing contaminants from optical surfaces being developed under NASA Contract NAS8-26385. This active cleaning technique involves exposing contaminated surfaces to a plasma containing atomic oxygen or combinations of other reactive gases. The ACT device laboratory demonstration model incorporates, in addition to plasma cleaning, the means to operate the device as an ion source for sputtering experiments. The overall ACT device includes a plasma generation tube, an ion accelerator, a gas supply system, a r.f. power supply and a high voltage DC power supply.

The previous ACT experiments, under Contract NAS8-26385, were conducted at much higher gas flows and chamber pressures (10^{-3} to 10^{-2} torr) than those contemplated for the LDM. Consequently a major concern of this program was the development of a plasma tube which was operable at the desired lower gas flow and chamber pressure conditions (less than 10^{-4} torr). Two ACT plasma tubes were developed which were compatible with the desired conditions. An ACT device prototype, incorporating the plasma tube, was designed, fabricated and tested. This prototype served as a means of verifying the basic design concept and determining the requirements and specifications for the auxiliary systems involved in the LDM. Based on the prototype device tests, a design was established for the ACT Laboratory Demonstration Model.

The prototype test results indicate that the LDM, at the desired gas flow and chamber pressure, will be capable of producing a centerline ion flux on the order of 10^{13} ions/cm^2-sec in the sputtering mode, and a centerline atomic oxygen flux in excess of 10^{14} atoms/cm^2-sec in the plasma cleaning mode. Repeated tests showed that no measurable contaminant cleaning could

be produced in the plasma cleaning mode while operating at a chamber pressure less than 10^{-4} torr. However, operation at higher chamber pressures (10^{-3} to 10^{-2} torr) produced satisfactory cleaning as had been demonstrated in prior experiments.

These results suggest that additional studies should be performed before finalizing the plasma tube design. These studies would be aimed at developing a plasma tube design and operational mode which would provide the appropriate active species to a contaminated surface.

2.0 INTRODUCTION

The need for developing an in-situ or active cleaning technique (ACT) for use in both space and vacuum chambers has recently become apparent. Manned spacecraft have experienced numerous contamination problems including deposition of volatile organic compounds onto windows, and light scattering from particulate contaminants surrounding the spacecraft. Sources of this contamination include outgassing of organic compounds, waste and water dumps, rocket plumes, and leakage from the life support system. It is believed that contaminant film deposition has also occurred on unmanned spacecraft surfaces. Data from a reflectometer experiment on the ATS-3 spacecraft (Reference 1) has indicated rather severe degradation on reflective surfaces, which may be the result of contaminant film deposition. Also, the TV camera mirror from the Surveyor III spacecraft which resided on the moon for 2-1/2 years was covered with a diffuse coating--presumably the result of contaminant film deposition. Contamination of an unmanned spacecraft has been verified with quartz-crystal thin film monitors on OGO-6 (Reference 2). A recent review of the spacecraft contamination problem has been published in Reference 3.

Contamination can also occur during spacecraft testing in high vacuum chambers. A recent example of this was the extreme-UV solar spectroheliometer experiment for the Apollo Telescope Mount (ATM) vehicle. A film of back-streamed diffusion pump oil was apparently deposited on surfaces during thermal/vacuum testing (Reference 4). Another example of contaminant film deposition during environmental testing is discussed in Reference 5. In those experiments it was shown that an extremely stable organic film could be deposited onto telescope mirror surfaces during irradiation with low energy protons in a relatively clean vacuum environment.

Based on existing knowledge, contamination problems anticipated for future spacecraft include: (1) deposition of non-volatile substances onto optical components, sensing elements, and temperature control surfaces; (2) particulate and gaseous contamination near the spacecraft (resulting in

light scattering and absorption); and (3) chemical contamination which can interfere with upper atmosphere studies, analysis of interplanetary or planetary matter, and material processing experiments. It is anticipated that contamination effects can be reduced by changes in design, materials, operating procedures, and possibly control techniques. The use of more sensitive surfaces and longer term missions will, however, offset these improvements. Thus, the need exists for developing an ACT for space use.

Experiments reported in References 5 and 6 have shown that exposure to a plasma containing atomic oxygen or combinations of other reactive gases is a very effective means of removing hydrocarbon contaminant films from optical surfaces in a vacuum. Although the detailed mechanisms of this cleaning process have not been investigated, it is believed that the oxidizable organic contaminant films are converted to volatile produces such as CO_2 and H_2O which subsequently evaporate in vacuum. An existing program "Active Cleaning Technique for Removing Contamination from Optical Surfaces in Space" (NASA Contract NAS8-26385) is continuing the investigation of using plasma cleaning as an active cleaning technique. The success obtained using plasma cleaning has led to the present program which is the development of a laboratory demonstration model (LDM) of an ACT device. This ACT device is to be matched to the NASA facility requirements and will incorporate the means for both plasma cleaning and sputtering mode operation.

3.0 PLASMA TUBE DEVELOPMENT

3.1 Design Concept and Preliminary Considerations

The basic design concept for the ACT device plasma tube is shown in Figure 1. The plasma tube consists of two concentric quartz tubes with the concentric annulus sealed at the downstream end. The radiofrequency (r.f.) electrodes are placed in the annular region near the downstream end to produce the plasma discharge in the gas just before it is exhausted into the vacuum. The electrodes are maintained at ambient pressure and an 'O' ring is used to seal the outer tube to the vacuum flange. The reactive gas flow rate is controlled by means of a restriction (capillary) at the downstream end of the inner tube.

This basic design concept is similar to the plasma tube design used in prior experiments (under Contract NAS8-26385) except for the addition of the flow restriction at the downstream end of the tube. In these prior experiments the primary emphasis was on the plasma cleaning effects rather than on the means of obtaining the plasma. The plasma tube used in prior experiments consisted of a 6 mm I.D. outer quartz tube, a 'straight through' 4 mm I.D. inner quartz tube and diametrically opposed tungsten wire or strip electrodes in the annulus. This tube was operated at a nominal pressure of 4 torr at the inlet and an oxygen flow rate of 50 std cc/min. The vacuum chamber pressure at this flow rate was about 10^{-3} torr. Under these conditions the plasma discharge resulted in what may be called the 'ignited plume' mode of operation. In the 'ignited plume' mode of operation the plasma discharge occurs both in the plasma tube and in a localized plume extending beyond the downstream end of the plasma tube. In this mode of operation there is also a 'chamber discharge' phenomena (i.e., a slight glow throughout the vacuum chamber).

The ACT device plasma tube must operate at both a much lower flow rate and vacuum chamber pressure than the plasma tube used previously. The first NASA LDM test facility will use a nominal 400 liter/sec Varian noble ion

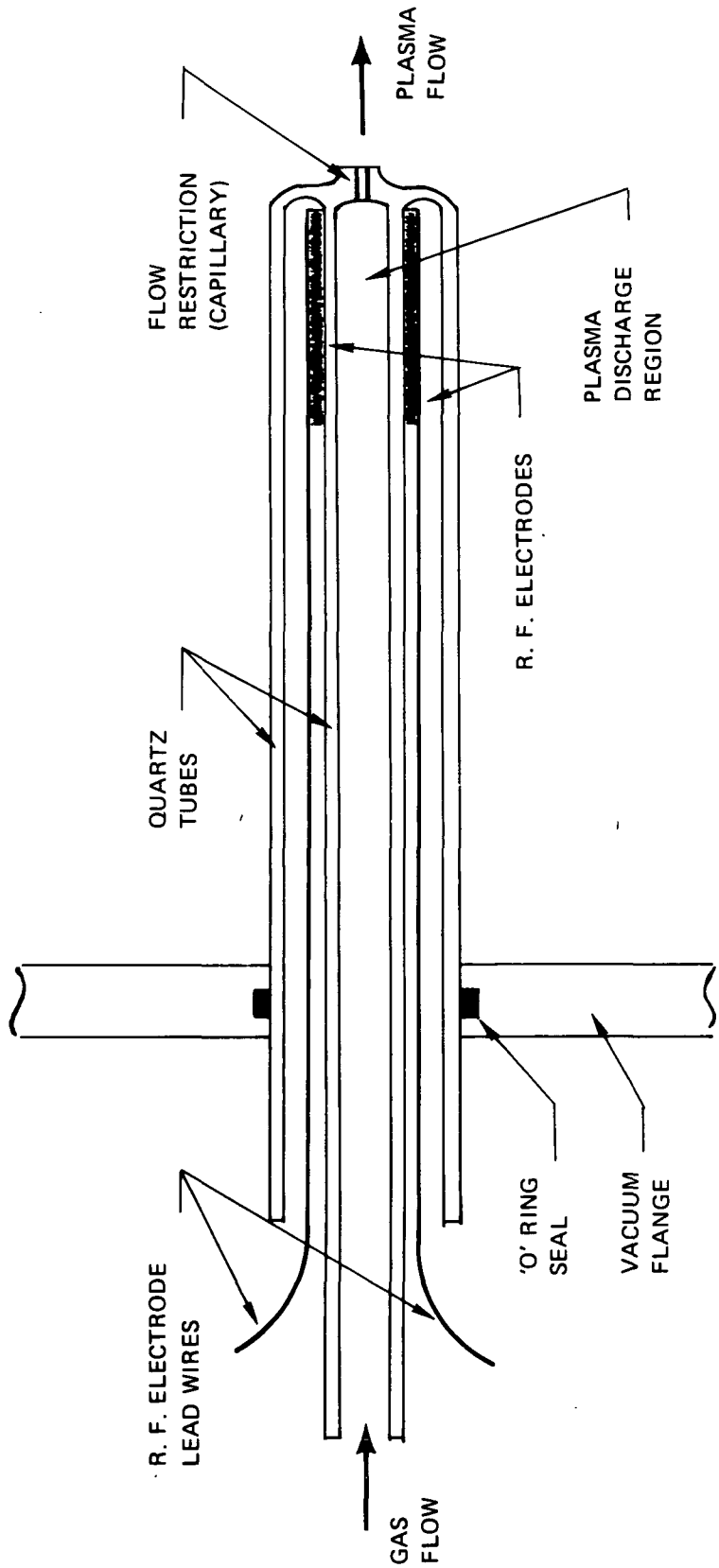

Figure 1 : Basic Design Concept For Act Plasma Tube

pump. This limits the oxygen flow rate to 0.18 std cc/min for a maximum vacuum chamber pressure of 10^{-5} torr. With the previous plasma tube design and the available r.f. power supply, the ignition of the plasma discharge requires a gas pressure of 2 to 20 torr. An initial checkout of plasma tube operation at low chamber pressure ($\sim 10^{-5}$ torr) was performed by adding a long capillary (nominally 0.02 cm dia x 2 cm length) to the previous plasma tube design. Tests of this plasma tube design showed that a plasma discharge could be sustained in the plasma tube at a chamber pressure of 10^{-5} torr. At this chamber pressure there was no 'chamber discharge' or 'ignitied plume' phenomena. At higher chamber pressures (10^{-3} torr) the 'chamber discharge' was observed both with and without the 'ignited plume' phenomena. Preliminary cleaning experiments using this modified plasma tube indicated cleaning of soot coated specimens. (It was later discovered that this apparent plasma cleaning was in reality caused by the high velocity gas stream, exhausting from the capillary during rapid chamber pumpdown, impinging on the specimen and blowing the soot off). It was believed that the long capillary used on this plasma tube would cause needless attenuation of the atomic oxygen. Therefore further design studies were undertaken to determine a more efficient plasma tube design for the ACT device.

3.2 Capillary Sizing Studies

The gas flow rate through the capillary depends on the plasma tube pressure, gas properties and the capillary dimensions. The gas flow rate may be written in terms of the plasma tube pressure as

$$Q = 0.079\left(\frac{T_s}{T}\right) pF \qquad (1)$$

where

Q = flow rate, STD cc/min

T_s = standard temperature, 273°K

T = gas temperature, °K

P = plasma tube pressure, torr

F = flow conductance of capillary, cc/sec

The flow conductance (F_v) for Poiseulle flow in a capillary is given by

$$F_v = \frac{\pi a^4}{8\mu\ell} P_a \tag{2}$$

where P_a = average pressure in capillary
a = capillary radius
ℓ = capillary length
μ = gas viscosity

The flow conductance (F_t) for molecular flow in a capillary is given by

$$F_t = \frac{2\pi a^3}{3\ell} \bar{v} \tag{3}$$

where

$\bar{v}$ = mean thermal velocity of gas molecules

$$= \left(\frac{8}{\pi} \frac{P}{\rho}\right)^{\frac{1}{2}}$$

ρ = density

The flow conductance (F_o) for molecular flow through an orifice of radius a is given by

$$F_o = \frac{\pi a^2}{4} \bar{v} \tag{4}$$

The flow conductance (F') for transitional flow in a capillary may be written (Reference 7) as

$$F' = F_v + Z F_t \tag{5}$$

where

$$Z = \frac{1 + 2.507\ a/\lambda a}{1 + 3.095\ a/\lambda a}$$

λ_{P_a} = mean free path corresponding to average pressure P_a

Considering the total flow resistance to be that of the capillary plus that of the open end (i.e., $1/F = 1/F' + 1/F_o$) the flow conductance may be written as

$$\frac{F}{F_t} = \frac{F_v/F_t + Z}{1 + (F_t/F_o)(F_v/F_t + Z)} \tag{6}$$

The flow conductance may be found in terms of plasma tube pressure, capillary dimensions and gas properties by using equations (2), (3) and (4) in equation (6) while noting that the average pressure in the capillary is given by $P_a = \frac{1}{2} P \left(1 + \frac{F}{F_o}\right)$ and that kinetic theory gives the viscosity as $\mu = 0.499\, \rho\, \bar{v}\, \lambda$. The resulting expressions for the parameters in equation (6) are:

$$\frac{F_v}{F_t} = \frac{0.0736}{\lambda_o} \left(\frac{T_s}{T}\right) \left(1 + \frac{8a}{3\ell} \frac{F}{F_t}\right) ap$$

$$Z = \frac{1 + \frac{2.507}{2\lambda_o} \left(\frac{T_s}{T}\right) \left(1 + \frac{8a}{3\ell} \frac{F}{F_t}\right) ap}{1 + \frac{3.095}{2\lambda_o} \left(\frac{T_s}{T}\right) \left(1 + \frac{8a}{3\ell} \frac{F}{F_t}\right) ap} \tag{7}$$

$$\frac{F_t}{F_o} = \frac{8a}{3\ell}$$

where λ_o = mean free path at 1 torr pressure and 273°K

$= 4.81 \times 10^{-3}$ cm for molecular oxygen.

The value for F/F_t can be obtained using the above expressions in an iterative solution to equation (6). The gas flow rate egn (1) can then be written as

$$Q = 7.13 \times 10^3 \left(\frac{32}{M} \frac{T_s}{T} \right)^{1/2} \left(\frac{a^3 p}{\ell} \right) \left(\frac{F}{F_t} \right) \qquad (8)$$

where M = molecular weight of gas.

Oxygen flow rates at 20°C were calculated, using eqn. 8, as a function of pressure for various capillary dimensions. Figure 2 gives the capillary sizing required for an oxygen flow rate 0.18 STD cc/min as a function of plasma tube pressure.

In addition to the plasma tube pressure, the atomic oxygen recombination on the capillary walls must be considered in the sizing of the capillary. The change in atomic oxygen concentration along the capillary may be written (assuming no radial variations) as

$$\frac{dN}{dX} = - \frac{\gamma \bar{v}}{2av} N \qquad (9)$$

where N = atomic oxygen concentration
X = distance along capillary
γ = atomic oxygen recombination coefficient on the capillary wall
$\bar{v}$ = mean thermal velocity of atomic oxygen
a = capillary radius
v = axial gas velocity

Assuming Poiseulle flow* equation (9) can be integrated to give

$$\ln \frac{N}{N_o} = - \frac{\gamma \bar{v} \ell}{3av_o} \qquad (10)$$

where subscript o refers to conditions at the upstream end of the capillary.

*Molecular flow would give factor of 1/4 instead of 1/3 in eqn. (10) and non-accelerating (constant density) flow would give factor of 1/2.

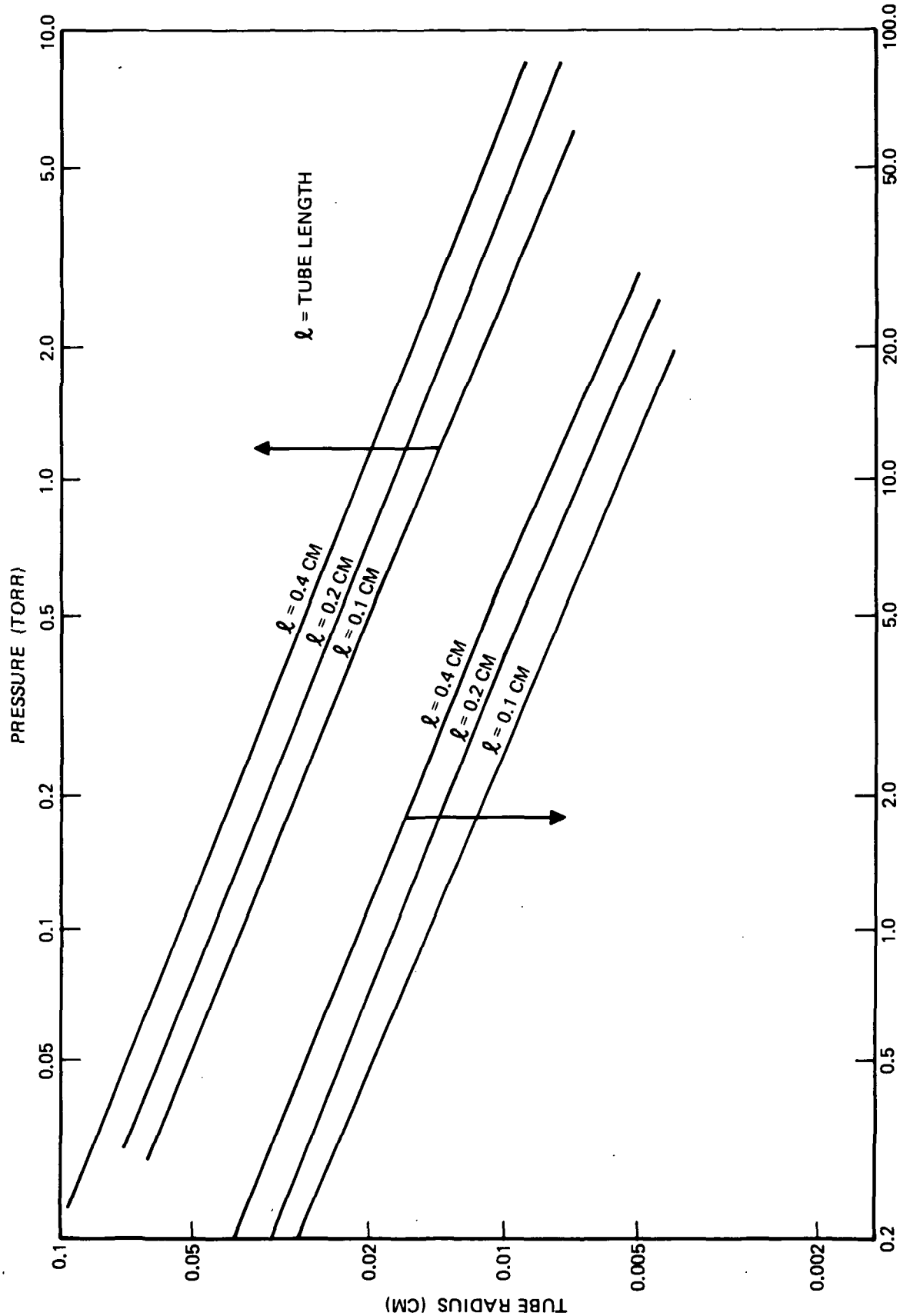

Figure 2: CAPILLARY TUBE SIZING FOR OXYGEN FLOW RATE OF 0.18 STD CC/MIN

Equation (10) may be expressed in terms of flow rate and plasma tube pressure (at 20°C) as

$$\ln \frac{N}{N_o} = -0.53 \times 10^4 \quad \frac{\gamma a \ell p}{Q} \tag{11}$$

where P = plasma tube pressure torr

Q = flow rate STD cc/min

Most of the reported values for γ range from 2×10^{-5} to 2×10^{-4} for atomic oxygen recombination on pyrex, silica and quartz at 20°C (reference 8). Using the upper value of 2×10^{-4} gives

$$\ln \frac{N}{N_o} = -1.06 \quad \frac{a \ell p}{Q} \tag{12}$$

Figure 3 shows the atomic oxygen attenuation expected at a flow rate of 0.18 STD cc/min for various capillary dimensions as a function of plasma tube pressure. The plasma tube used in the previous experiments operates at a pressure of about 4 torr, therefore the added capillary should have a radius of 0.01 cm or less in order to minimize the atomic oxygen attenuation (see Figure 3). However, the fabrication of a quartz tube with a small diameter capillary appears to present a difficult and costly problem. Consequently, it was decided to investigate the possibility of having a lower pressure plasma discharge which would allow the use of a larger diameter capillary.

3.3 Plasma Discharge Tube Sizing

The inability of the previous plasma tube to sustain a discharge at lower pressures was thought to be due to the electron oscillation amplitude limit. This limitation on the discharge arises when the electron oscillation amplitude becomes so large that the electrons are all swept to the plasma tube walls on each half cycle.

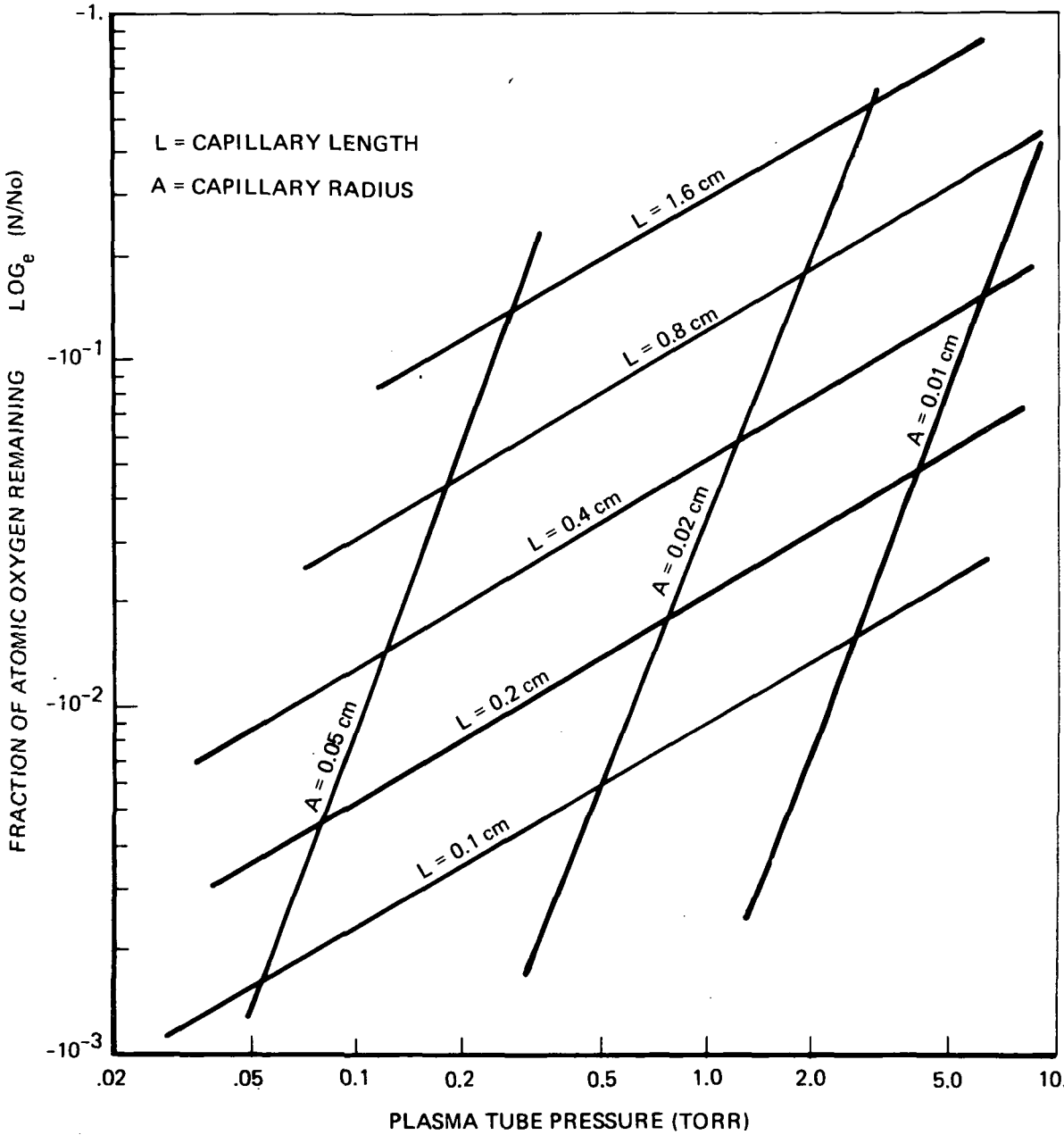

Figure 3 : Atomic Oxygen Attenuation in Plasma Tube Capillary for a Flow Rate of 0.18 STD CC/MIN and Recombination Coefficient of 2×10^{-4}

In a uniform alternating electric field the amplitude of the electron oscillations is given by

$$X = \frac{e}{m} \quad \frac{E}{2\pi f} \quad \left[(2\pi f)^2 + V^2\right]^{-1/2} \tag{13}$$

where E = peak electric field strength

e/m = charge to mass ratio for electrons

f = frequency of applied electric field

V = electron collision frequency with gas molecules

For the case when $(2\pi f/V)^2 << 1$, equation (13) may be written

$$X \simeq \frac{e\ E/m}{2\pi f V} \tag{14}$$

Since the collision frequency is approximately proportional to the pressure, the electron oscillation amplitude limit may be overcome at lower pressures by increasing the plasma tube size or by increasing the applied frequency.

The effect of plasma tube size on the breakdown voltage characteristics was experimentally determined by measuring the breakdown voltage as a function of pressure for three tubes of different diameter (and electrode spacing). The results of these measurements are shown in Figure 4. The 4 mm I.D. tube was the plasma tube used in the previous experiments. The larger size tube measurements were made using lengths of 0.25 inch diameter copper tubing, attached diametrically opposed on the outside of the tubes, as the electrodes. Figure 4 shows that the larger tubes, in addition to being operable at lower pressures, result in a much lower breakdown voltage.

The effect of frequency on the plasma tube voltage versus pressure characteristics was experimentally determined for a 17 mm I.D. tube using the copper tubing electrodes. The voltage measurements were made for frequencies ranging from 10 to 44 MHz. Figure 5 shows the breakdown voltage and minimum

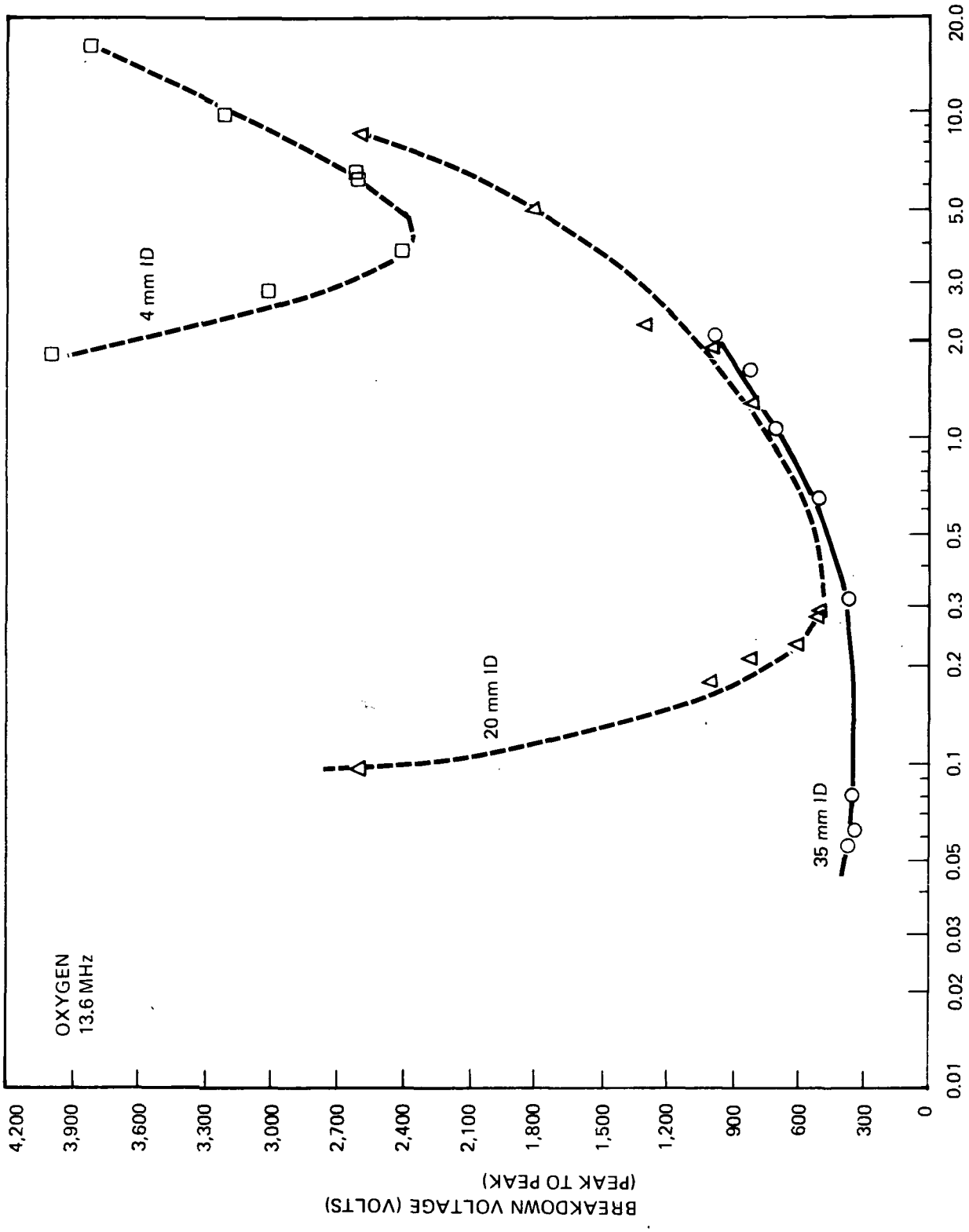

Figure 4 : Effect of Plasma Tube Size on Breakdown Voltage

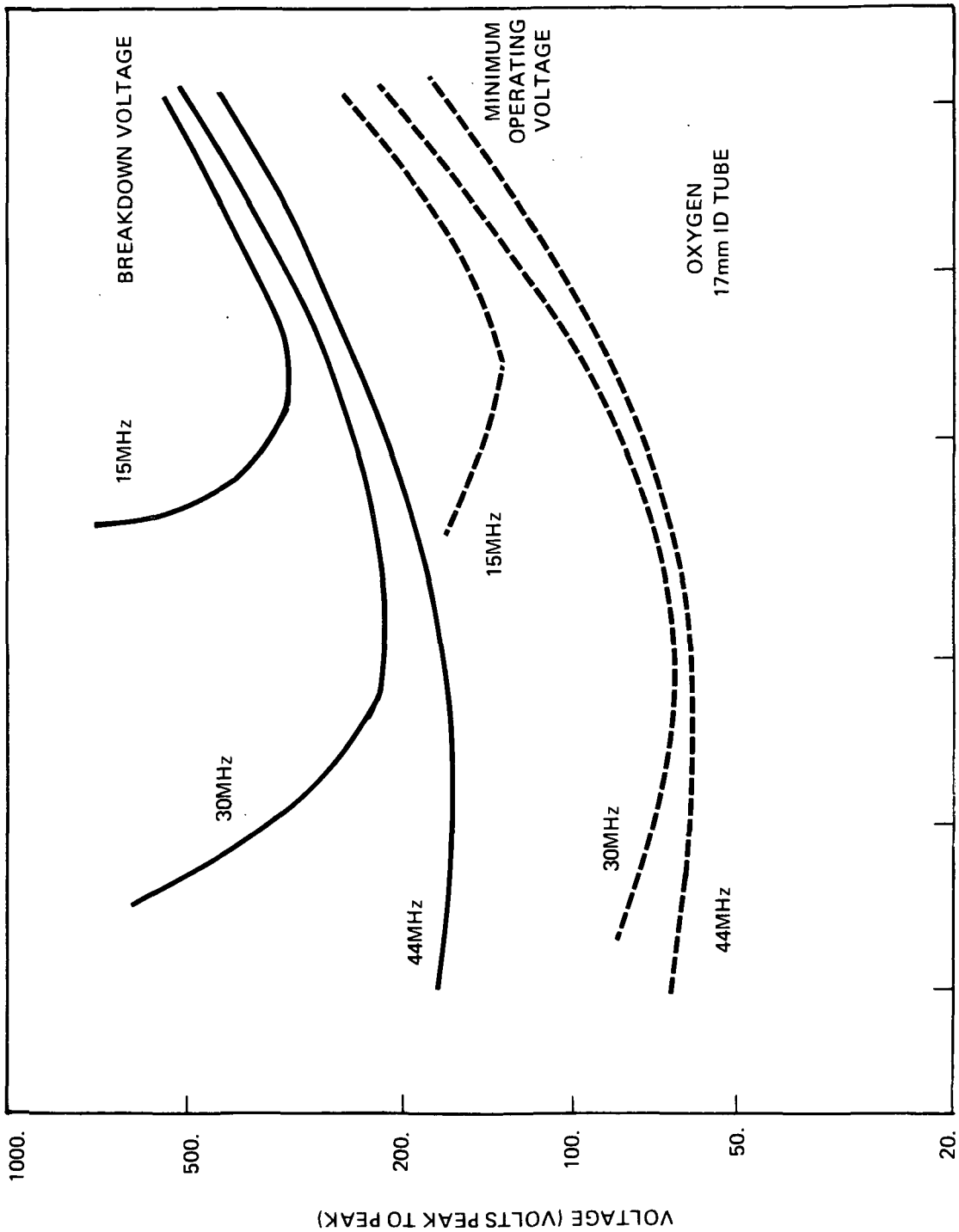

Figure 5 : Effect of Frequency on Plasma Discharge Voltage

operating voltage as a function of pressure for frequencies of 15, 30 and 44 MHz. These results show that the voltages and operating pressures are reduced as the frequency is increased.

3.4 ACT Plasma Tube Design

Based on the capillary and discharge tube sizing studies, the available quartz tube sizes, and the available space on the vacuum flange assembly to be used in mounting the ACT device to the vacuum system, two plasma tubes were designed and fabricated. These two plasma tubes are identical, with the exception of the capillary dimensions. Both plasma tubes consist of a 30 mm I.D. outer tube and a 17 mm I.D. by 10 cm length inner plasma discharge tube. The inner and outer tubes are sealed together at the downstream end. An 8 mm I.D. gas supply tube is sealed into the upstream end of the plasma discharge tube. A short section of 4 mm I.D. tube is sealed to the upstream end of the gas supply tube to provide a connection to the gas supply system. The capillary, drilled in the downstream end of the plasma discharge tube, was sized to give the desired gas flow rate at a given discharge tube pressure. Plasma Tube No. 1 has a 0.05 cm dia by 0.2 cm length capillary calculated to give an oxygen flow rate of 0.18 STD cc/min at a pressure of 0.43 torr. Plasma Tube No. 2 has a 0.1 cm dia by 0.4 cm length capillary calculated to give an oxygen flow rate of 0.9 STD cc/min at 0.48 torr.

Figure 6 shows one of these plasma tubes along with a Teflon end plug support and the assembled electrodes. The electrodes were cut from aluminum tubing and formed to fit the outside of the discharge tube. Teflon rings were used to hold the electrodes in position. Figure 7 shows an assembled plasma tube and Figure 8 shows a closeup view of the capillary in Plasma Tube No. 2. These plasma tubes were used in the ACT device prototype.

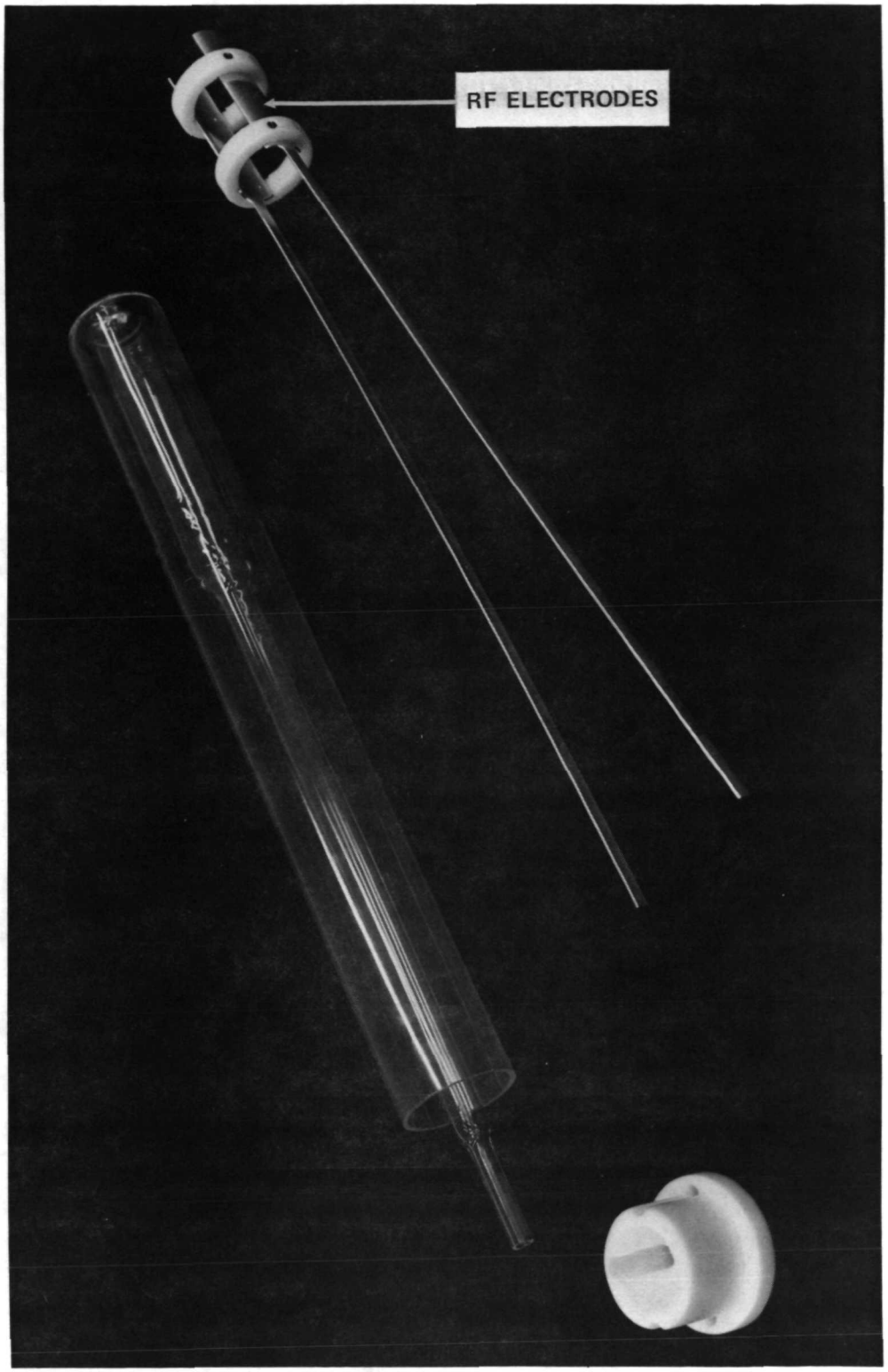

Figure 6 : Plasma Tube Components

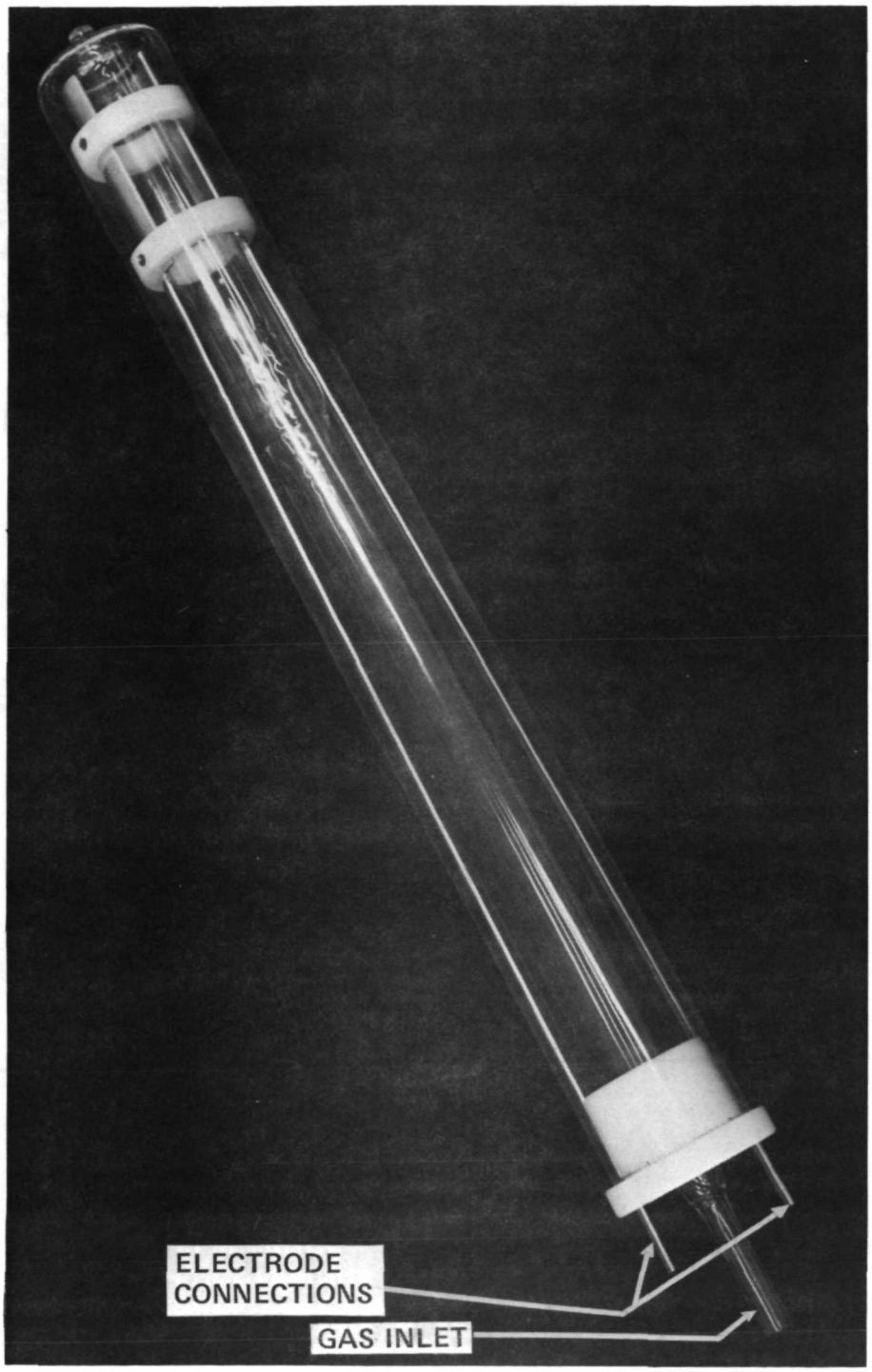

Figure 7 : Assembled Plasma Tube

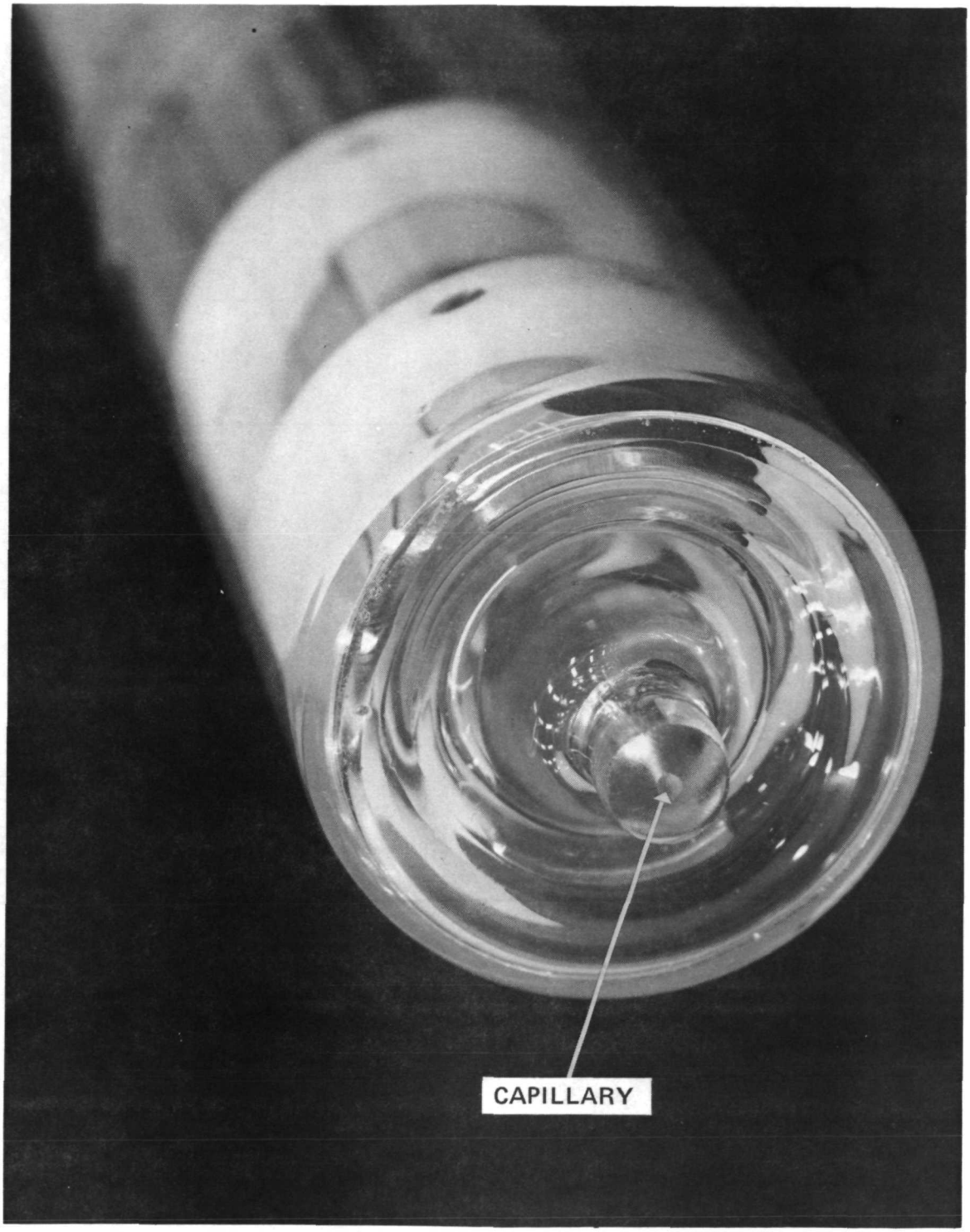

Figure 8 : Plasma Tube No. 2 – Capillary

4.0 ACT DEVICE PROTOTYPE

A prototype of the ACT Device LDM was designed, fabricated and tested. The basic device (shown in Figure 9) consists of the plasma tube assembly, vacuum flange, r.f. shielding tube and a Gap-Einzel lens assembly. The LDM includes, in addition to this basic device, a gas supply system, a r.f. power supply system, a high voltage supply system and a control console. The prototype of the ACT Device served as a test bed for determining the requirements and specifications for these auxiliary systems, as well as a means of verifying the performance of the basic design concept.

Figure 9 shows the basic device in the configuration for the sputtering mode of operation. The plasma is biased to a given potential by means of a probe wire which contacts the plasma discharge. The anode/extractor extracts the electrons from the plasma as it leaves the capillary, the remaining ions are accelerated and focused as they pass through the lens system. With the Gap-Einzel lens assembly removed, the basic device is in the plasma cleaning mode configuration. In this configuration the active plasma species leaving the capillary are available for plasma cleaning purposes.

4.1 Plasma Cleaning Mode Tests

The prototype ACT device was tested in the plasma cleaning mode configuration using oxygen. The primary purpose of these tests was to determine the atomic oxygen flux produced by the ACT plasma tubes. Subsidiary purposes of these tests were the verification of the plasma tube operation under low flow rate and pressure conditions, as well as, the verification of the gas supply system operation. The prototype device configuration used in these tests is shown in Figure 10. A "leak valve" (Granville Phillips type 203) for flow control is shown mounted on a clear plastic plate which is attached by studs to the vacuum flange. The gas flows from this valve through Teflon tubing to a 'tee' fitting that is connected to the gas supply tube of the ACT plasma tube. The open end of the 'tee' connects to a pirani gauge tube (not shown). Also shown in Figure 10 is the catalytic probe assembly which passes through the flange and has the probes positioned downstream of the plasma tube

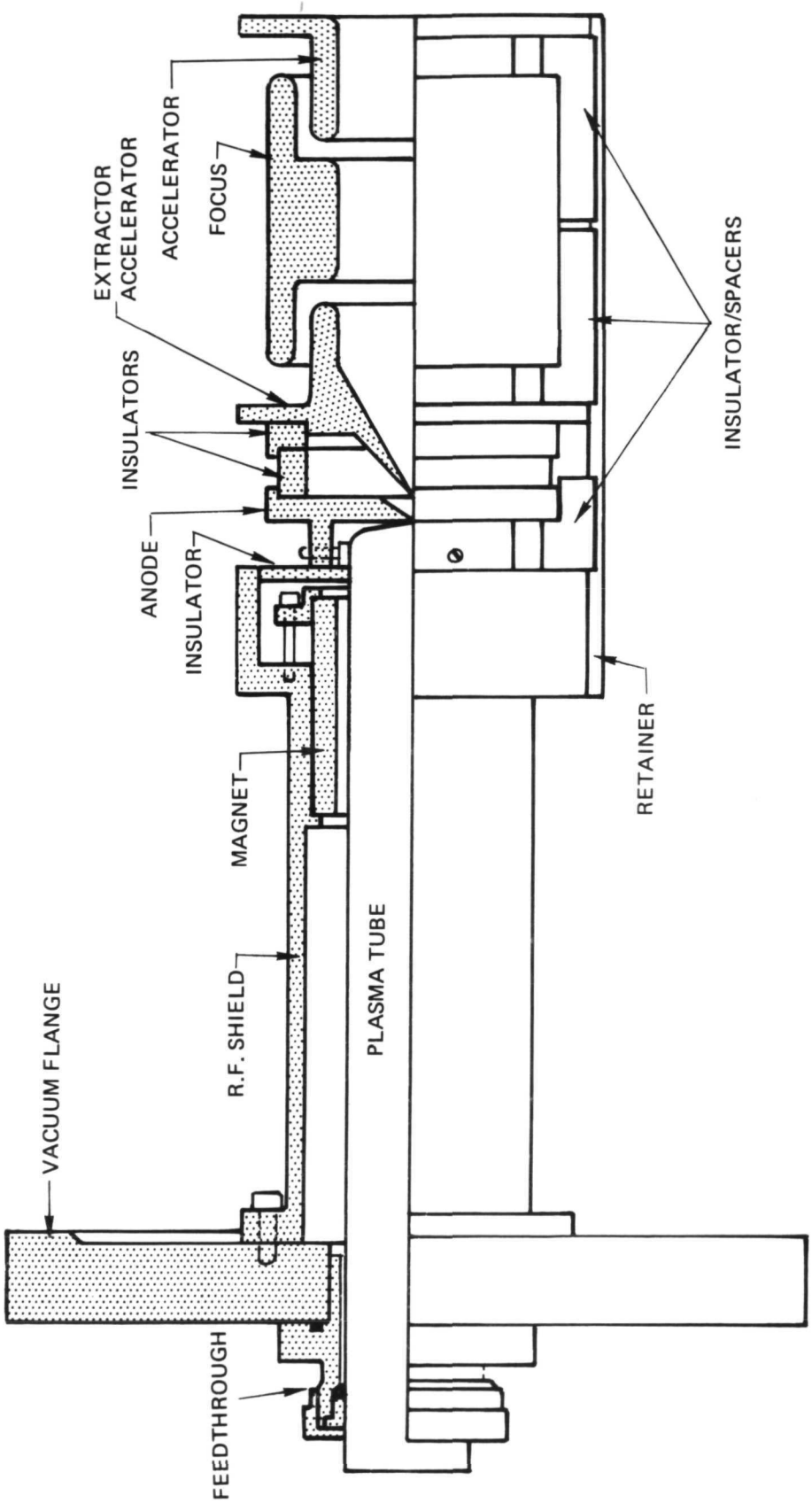

Figure 9: PROTOTYPE ACT DEVICE WITH GAP/EINZEL LENS ASSEMBLY

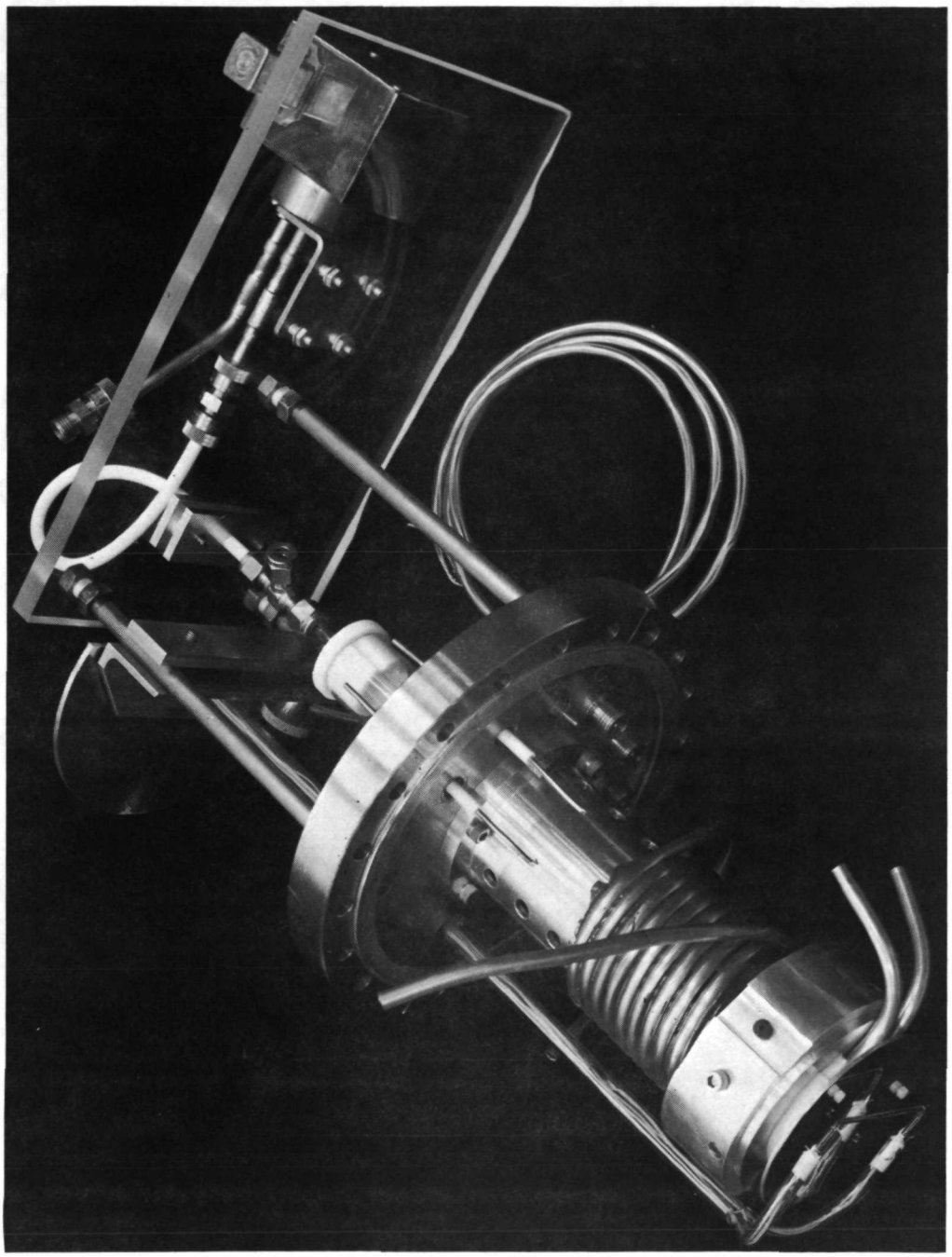

Figure 10 : Prototype Act Device

capillary. This catalytic probe is discussed in Section 4.1.2. Figure 11 shows another view of the configuration without the plasma tube or catalytic probe assemblies in place. Electrical feedthroughs (two high voltage and five low voltage) are provided for the operation and test measurements using the ACT Device in the sputtering mode.

4.1.1 Gas Flow Rate Tests

Oxygen flow rates were measured at various plasma tube pressures for plasma tubes No. 1 and No. 2. These measurements were made by determining the rate of pressure decay in a pressurized reservior connected to the upstream side of the 'leak valve'. The prototype ACT device was mounted to a vacuum chamber in which the pressure was kept below 10^{-5} torr. Plasma tube pressure was maintained at a constant value during the measurements.

The flow rate measurement results are shown in Figure 12 for both plasma tubes. The calculated flow rate versus pressure curves for the two plasma tube capillaries are also shown in Figure 12. The agreement between the measured and predicted flow rates is within the fabrication tolerances of the capillaries and the accuracy limits of the plasma tube pressure measurements.

4.1.2 Catalytic Probe Tests

One means of determining the atomic oxygen flux produced by the ACT device plasma tubes is the measurement of heating caused by the recombination of atomic oxygen on a catalytic surface. Previous experimenters (reference 9) have reported good results using silver oxide as a catalytic surface. Development of a catalytic probe for use with the ACT devices was initiated during the previous work, under Contract NAS8-26385, and was continued under the present contracted effort.

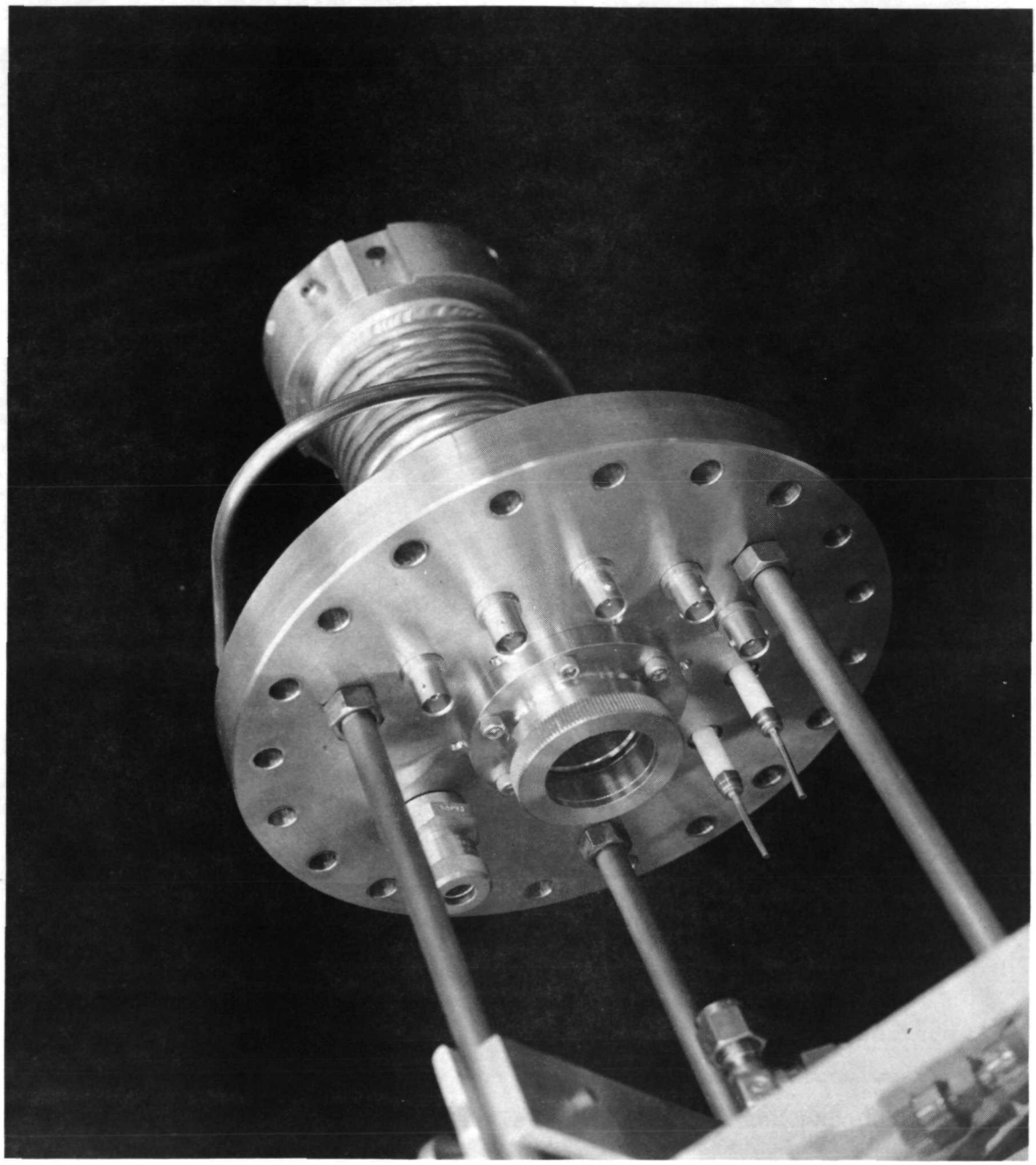

Figure 11 : Prototype Act Device

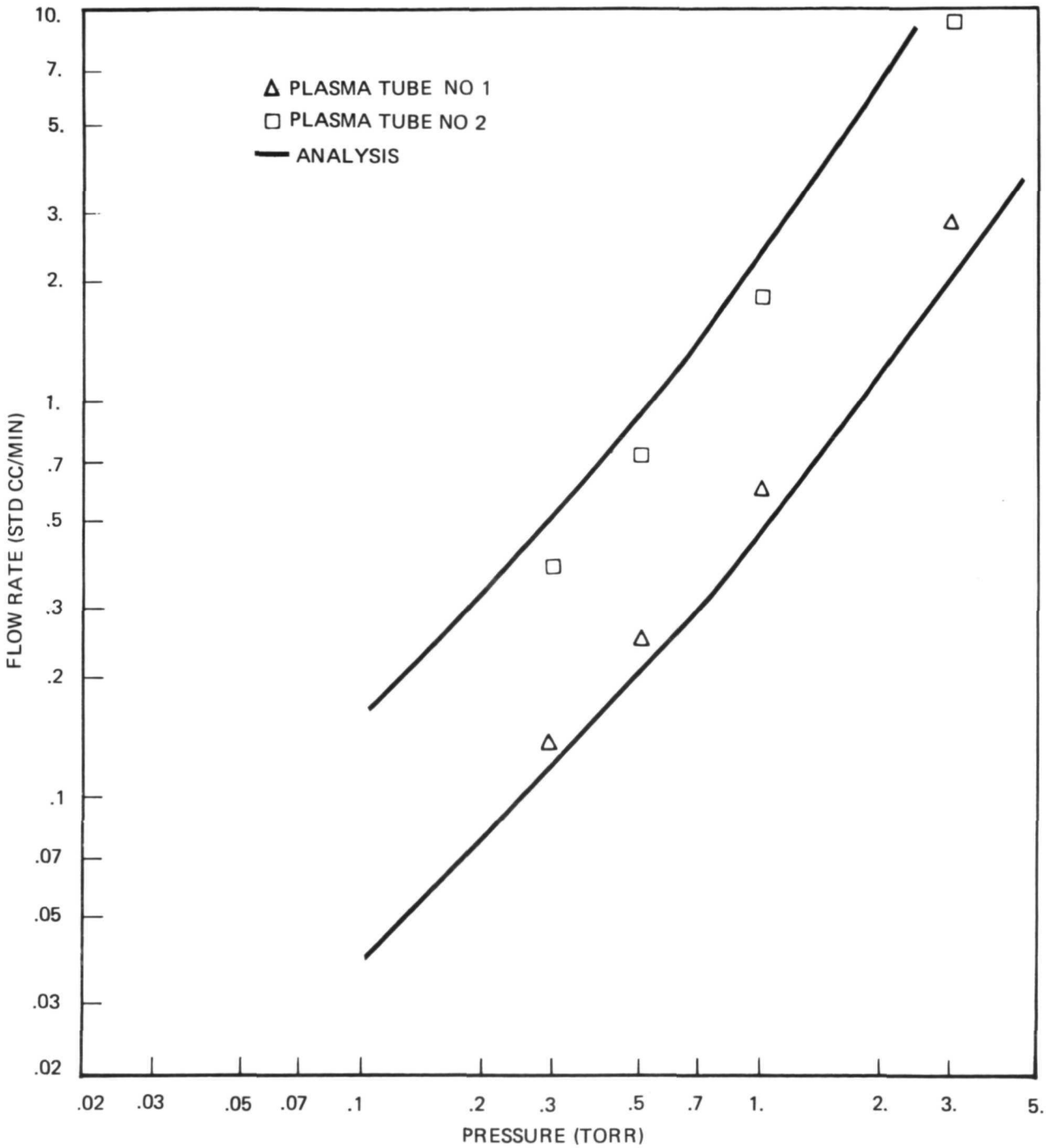

Figure 12 : Flow Rate Calibration

The catalytic probe assembly in the present effort used two thermistors, one with a catalytic surface and the other with a non-catalytic surface. The use of these two thermistors should allow the heating caused by factors other than oxygen recombination to be eliminated. The difference in heating between catalytic and non-catalytic surface thermistors gives a measure of the heating due to atomic oxygen recombination. The 'plasma heating' of each thermistor is determined by measuring the additional electrical power required to maintain the thermistor resistance (temperature) at the same value, with the plasma discharge discharge turned off, as it had with the plasma discharge turned on. The catalytic surface for the one thermistor was produced by coating the glass bead with silver and letting it oxidize in the plasma stream. The noncatalytic surface for the other thermistor was achieved by leaving the glass bead uncoated.

The catalytic probe assemblies first developed (under Contract NAS8-26385) did not prove satisfactory for the measurement of the atomic oxygen flux. One of the major problems with these early probe assemblies was the lack of adequate sensitivity. Subsequently, an analysis was made to determine the sensitivity required to measure the expected atomic oxygen flux. The expected heating rate due to atomic oxygen recombination on the catalytic thermistor, at a flow rate of 0.18 STD cc/min and a one percent atomic oxygen concentration, is on the order of 10^{-6} watts at 1 cm distance from the capillary exit assuming a diffuse flow pattern. The measurement of this low heating rate required more sensitivie instrumentation and further thermal decoupling of the thermistor bead from the probe assembly.

A new catalytic probe assembly was designed such that the thermal conductance between the thermistor beads and the environment would be on the order of 10^{-4} watts/°C or less. A closeup view of the thermistors mounted in the probe assembly is shown in Figure 13. Figure 14 shows a view of the entire probe assembly.

The relationship of the probe assembly to the ACT device assembly was shown earlier in Figure 10. The response characteristics for this catalytic probe

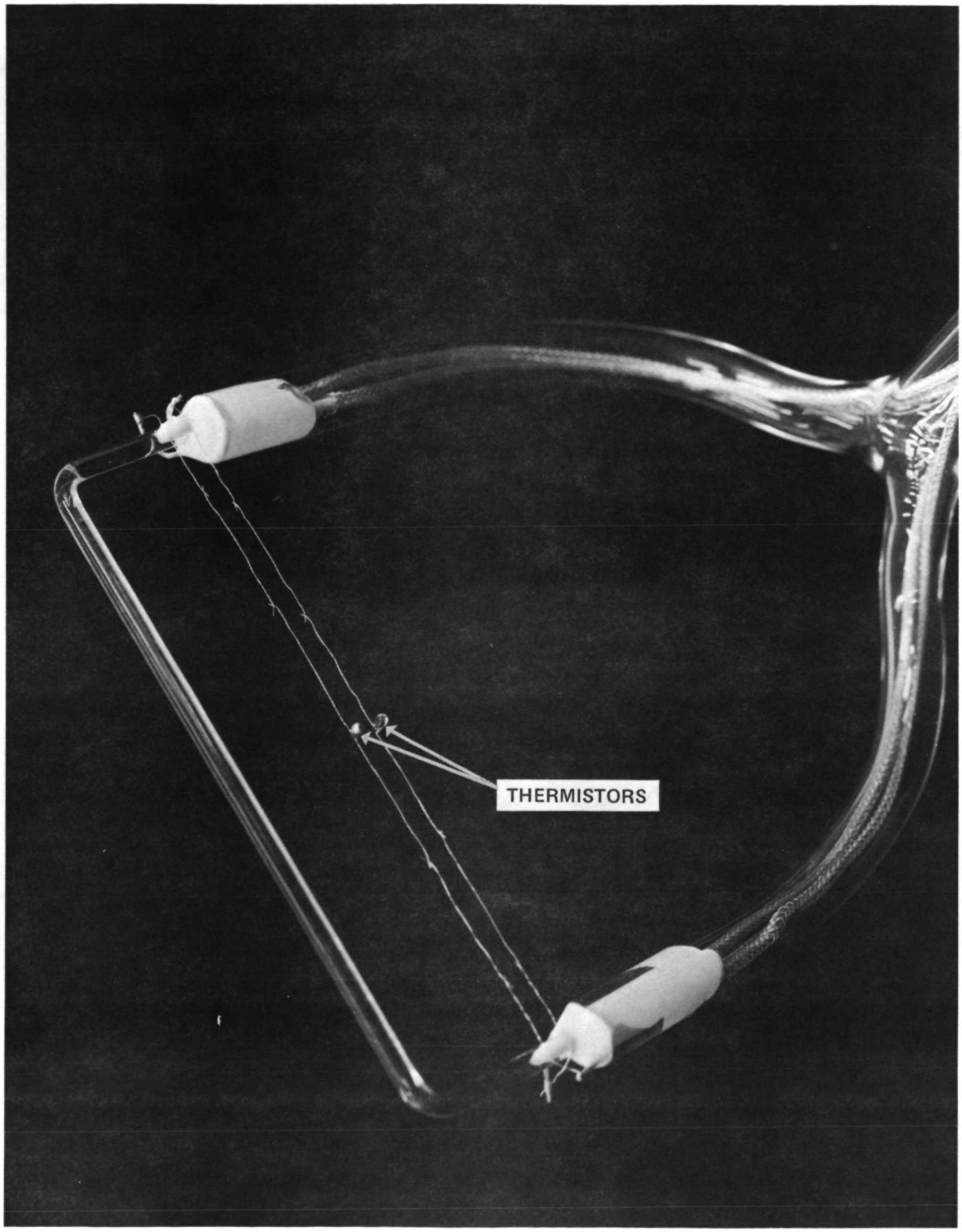

Figure 13: Thermistor Installation In Probe Assembly

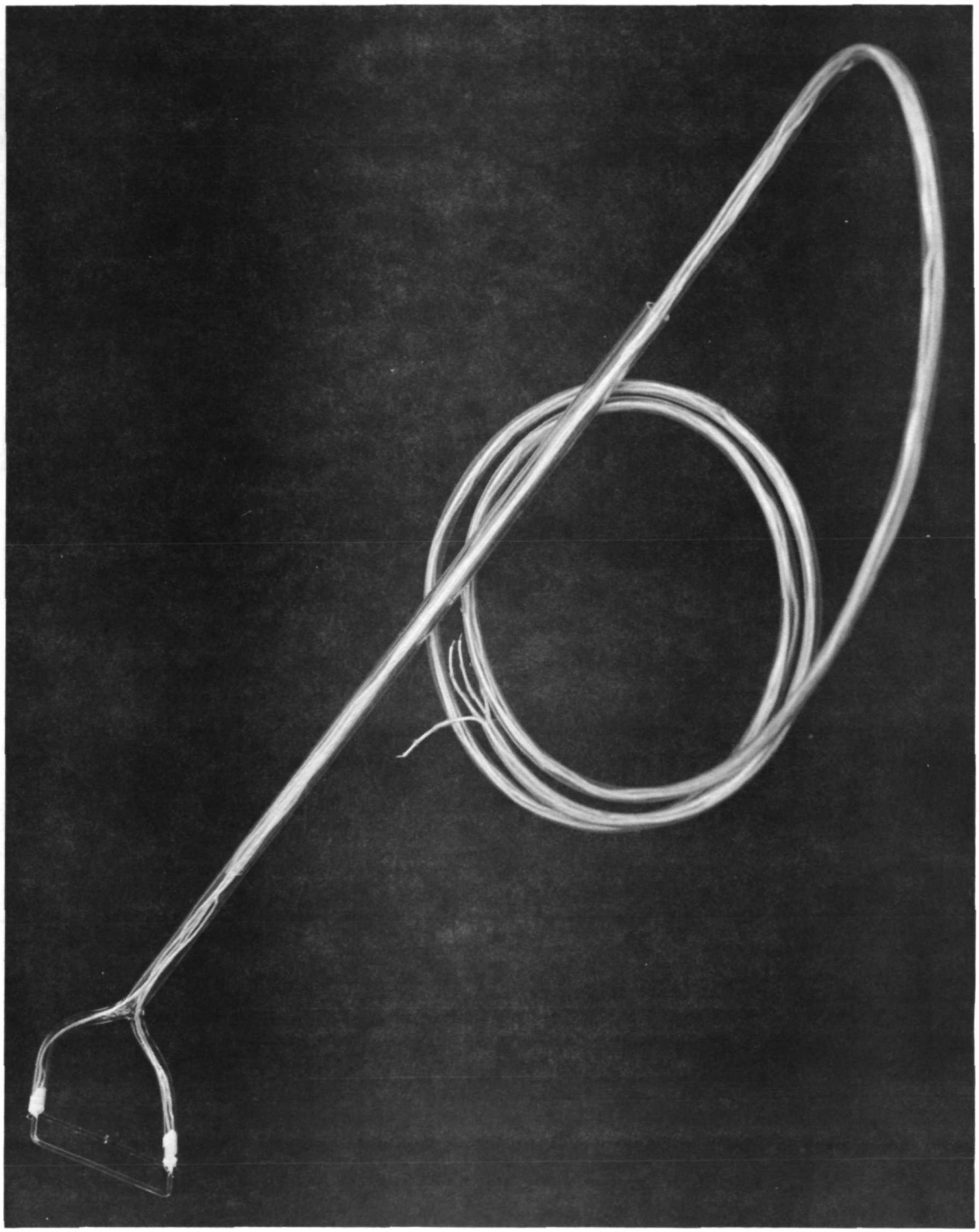

Figure 14 : Catalytic Probe Assembly

assembly were determined by measuring the thermistor resistances as a function of power input. The relationship between thermistor resistance and temperature may be written as

$$\frac{dR}{dT} = \alpha R \tag{15}$$

where R = resistance, ohms
T = temperature, °C
α = temperature characteristic, $(°C)^{-1}$

The relationship between power input and thermistor temperature can be written as

$$\frac{dQ}{dT} = K \tag{16}$$

where Q = power input, watts
K = effective thermal conductance, watts/°C

Using equations (15) and (16) the relationship between power input and thermistor resistance can be written as

$$\frac{dQ}{dR} = \left(\frac{K}{\alpha}\right) \frac{1}{R} \tag{17}$$

The (K/α) values determined for the probe assembly are shown in Figure 15 as a function of thermistor resistance. These results show that the probe assembly is sensitive enough to measure low heating rates since the response is on the order of 10^{-6} watts/ohm.

More sensitive instrumentation was acquired for the probe measurements. Analyses and checkout of this instrumentation showed that the heating rate could be determined to within about $\pm 10^{-7}$ watts. This accuracy may be somewhat marginal for a flow rate of 0.18 STD cc/min but should be adequate for flow rates on the order of 1 STD cc/min.

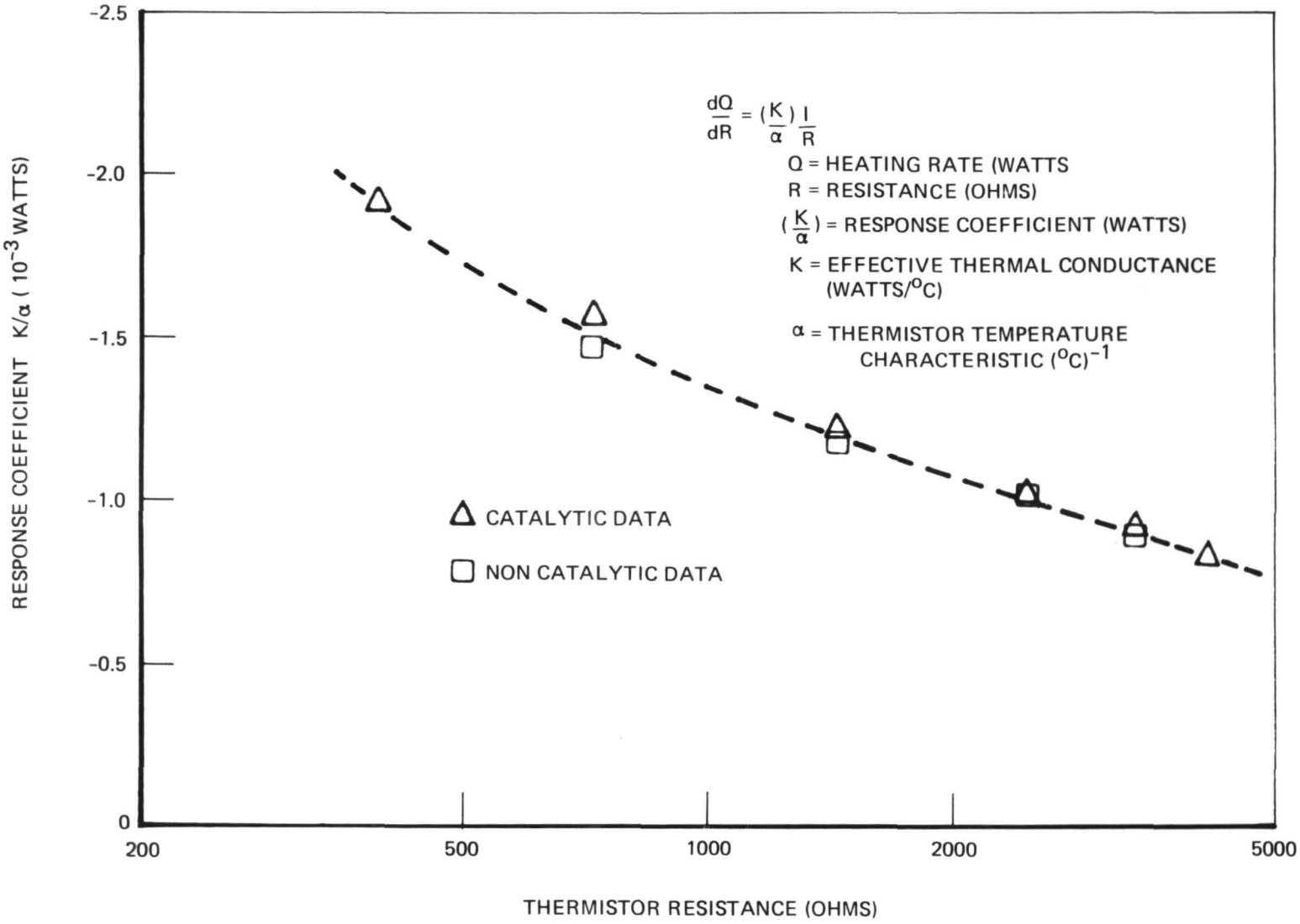

Figure 15 : Thermistor Response Characteristics

In addition to sensitivity requirements for the catalytic probe assembly and instrumentation, the 'background noise' must be low enough to allow probe measurements to be made. This background noise includes temperature variations in the surroundings and electrical interferences from the r.f. power system. To reduce background temperature variations, cooling coils were attached to the r.f. shielding tube. Tests with earlier probes had indicated that radiation from the plasma tube was heating the thermistor probes. Since the surface radiative properties of the two thermistors are different, this radiative heat source does not give identical heating on the two thermistors. The r.f. interference problems with the earlier probes were solved by proper shielding and grounding.

Initial tests with the new catalytic probe revealed some severe r.f. interference problems that precluded measurement of the probe response. Further testing showed that the thermistors were being heated by r.f. current generated in the lead wires. The thermistor temperatures increased by up to about 100°C. This heating effect was greatly reduced by 'short circuiting' the r.f. in the instrumentation circuitry with capacitors. However, even with the reduced r.f. heating of the thermistors, the temperature rise (about 1°C) was still too large to make accurate measurements of the probe response. It is believed that addition of capacitors across the thermistor leads, where they attach to the probe assembly, might reduce the r.f. heating to a point where measurements could be made. However, the uncertainty involved, and the lack of time and funds, precluded continuation of the probe development under the present effort.

4.1.3 Silver Oxidation Tests

Because of the problems involved in developing a suitable catalytic probe for determining atomic oxygen flux, silver-coated surfaces were used to determine the oxidization produced by the prototype ACT device. Silver surfaced mirrors were exposed to the plasma at various distances from the capillary to determine oxidation effects. The mirrors were 2 inch (5.08 cm) square samples with a just opaque silver coating. Four mirrors were tested

using Plasma Tube No. 2 in the prototype ACT device. Table 1 summarizes these tests. Mirrors numbered 2 and 4 are shown in Figure 16. These mirrors developed multicolored interference patterns in short exposure times, whereas the other two mirrors developed only grey spots after relatively long exposure times. The reason for these differences is not known, however, only the silver films which oxidized completely through exhibited the interference rings. In an attempt to get a quantitative measure of the silver oxidation pattern, two mirrors were coated with 1700-2600 Å of silver. During the silver coating operation, a strip was masked off across the center of the mirror to provide a reference plane for post test interferometry measurements which would provide data on the oxidation pattern thickness. The first mirror was exposed for 60 min. at 1.3 cm distance from the capillary. The oxygen flow rate was 1 STD cc/min, chamber pressure 5.8×10^{-5} torr and the peak to peak r.f. voltage was 1000 volts. The test results showed a circular grayish black spot about 2.5 cm dia., surrounded by a brownish colored ring. However, there appeared to be only a very slight oxidation of the silver just adjacent to the bare strip (that approximately bisected the overall circular oxidation pattern). Thinking that this might have been due to an electrical charge buildup phenomena on the strip of bare substrate, the second mirror was tested with only one half of the mirror surface grounded (the entire silver surface was grounded in the previous tests) while the other half was left floating (i.e., ungrounded). The test results for the second mirror were essentially the same as those for the first mirror. Consequently, it appears that grounding has little, if any, effect on the oxidation of silver. The reason for slower oxidation of silver near the edge of the coated area is not known. This effect may also be seen in Figure 16 for the mirror with the larger circular interference pattern. The side opposite to the uncoated edge on this mirror was masked by the sample holder, however, the truncation of the circular pattern along the other edges is similar to the effect observed for the two mirrors with the bare substrate strip through their centers.

In order to get a quantitative measure of the silver oxidation rate, tests were conducted using silver coated quartz crystals in a Quartz Crystal Microbalance (QCM). The frequency of the QCM depends on the mass added to

TABLE 1: SILVERED MIRROR TESTS

TEST RUN NO.	1	2	3	4	5	6
MIRROR NO.	1	2	3	4	1	1
DISTANCE FROM CAPILLARY (CM)	5.	1.3	2.5	2.5	2.5	2.5
RUN TIME (MIN.)	120.	5.	35.	6.	35.	20.
FLOW RATE (STD CC/MIN)	1.	1.	1.	2.5	1.	2.5
CHAMBER PRESSURE (TORR)	5×10^{-5}	7.6×10^{-5}	7×10^{-5}	2×10^{-4}	6.2×10^{-5}	2×10^{-4}
POWER INPUT (WATTS)	6.	5.	6.	5.	5.	5.
PEAK TO PEAK R.F. VOLTAGE (VOLTS)	1100	1100	1100	1100	1000	1100
RESULTS	No visible effects	Circular interference patterns in spot 2.2 cm dia.	Circular spot about 2.8 cm dia. No interference patterns	Circular interference patterns in spot 5 cm. dia.	No visible effects	Circular spot about 5 cm. dia. No interference patterns

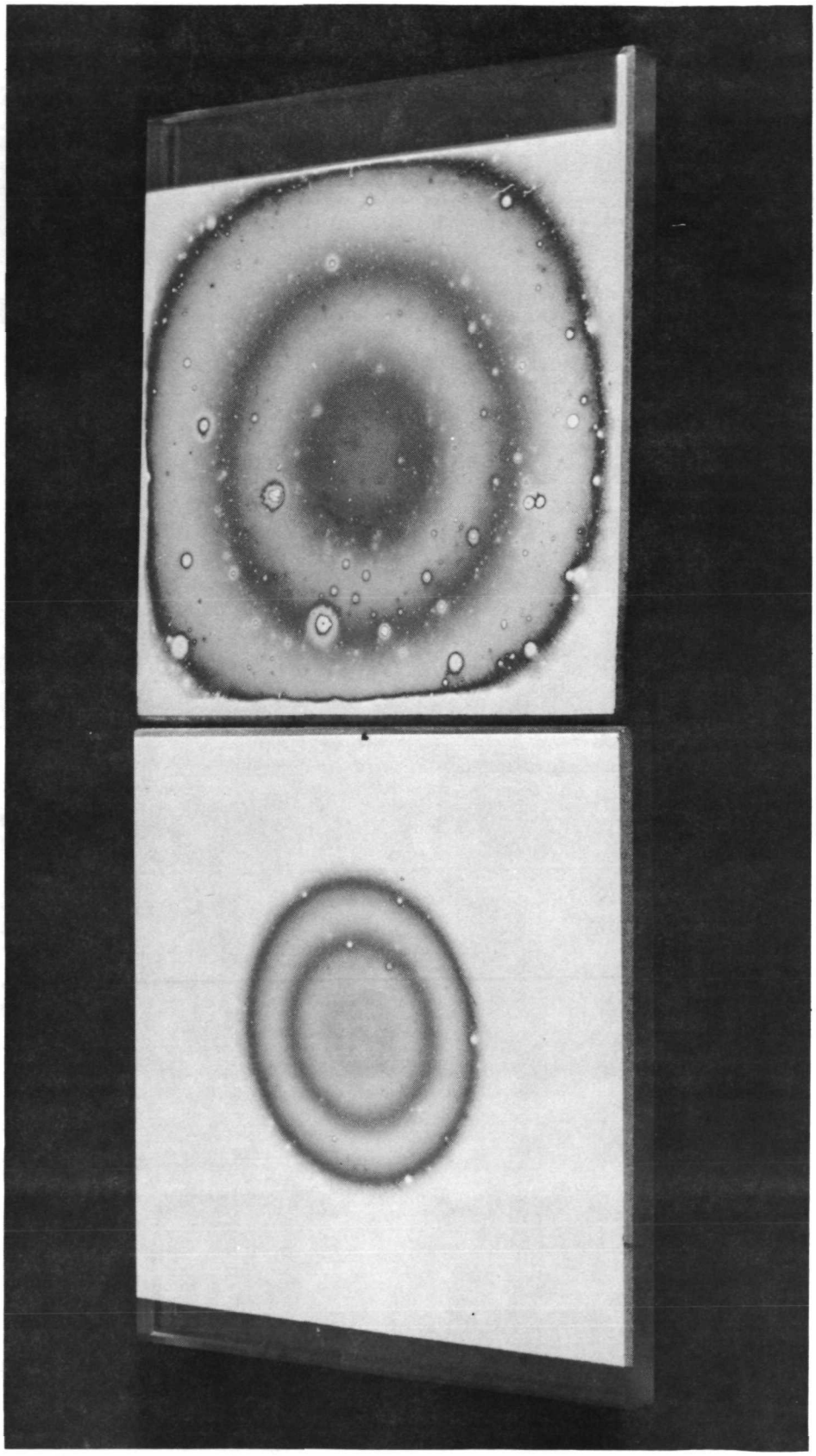

Figure 16 : Oxidized Silver Coatings On 5.08cm Square Glass Substrates

the quartz crystal surface. The greater the added mass the lower the frequency of oscillation. A Sloan Deposit Thickness Monitor (Model DTM-4) was used in conjunction with 5 MHz crystals (silver). Preliminary tests with the QCM holder mounted about 2.5 cm from the capillary showed that the silver oxidation produced a measureable frequency decrease as the silver oxidized. A new 5 MHz silver coated crystal was installed in the QCM holder and the frequency response was measured for various plasma operating conditions. The frequency was measured with a strip chart recorder attached to the DTM-4. The span on the chart was set to 400 Hz and when the frequency change neared the end of the chart span, the plasma discharge was turned off and the zero was reset on the chart prior to reinitiating the plasma discharge. The results of this test are summarized in Table 2.

After initiation (or reinitiation) of the discharge, the QCM frequency change appeared to be exponential with time until a linear rate of change was reached. (Table 2 gives this linear rate of frequency change.) The results in Table 2 show that the rate of frequency change drops off with run time and/or time elapsed between runs. The results also indicate that an optimum operating voltage exists at which the rate of frequency change is maximized. Also, as expected, the rate of frequency change is increased as the flow rate is increased.

To determine how the rate of frequency change varied with run time, a new silver coated crystal was installed in the QCM holder and the frequency response was measured without interruption of the plasma discharge conditions. The exposure was continued until the silver was completely oxidized. The plasma discharge operating conditions for this test were: r.f. peak-to-peak voltage of 1200 volts, oxygen flow rate of approximately 1 STD cc/min, and a vacuum chamber pressure of 7×10^{-5} torr. The QCM holder was positioned about 2.5 cm from the capillary. The frequency change as a function of plasma exposure time is shown in Figure 17. No frequency change was apparent until after about 6-7 minutes of exposure. The frequency change with exposure time appeared to be stabilizing to a value somewhat greater than 1300 Hz when, after about 57 minutes, stepwise reductions in the

TABLE 2: SILVER COATED QCM TEST RESULTS

Time Elapsed Before Reinitiation of Plasma Discharge (Minutes)	Plasma On-Time (Minutes)	Rate of Frequency Change (Hz/sec)	R.F. Peak to Peak Voltage (Volts)	Oxygen Flow Rate (Std cc/min)
N/A	3	1.63	1000	1.
22.	7.	0.95	470	1.
		0.76	1000	
		0.84	400	
		0.66	300	
20.	10.	0.35	1800	1.
		* 0.52-0.71	1000	
		0.69	500	
		0.58	700	
18.	8.	0.84	1100	2.5
		0.46	1500	
		0.81	500	

*Plasma operation somewhat unstable while tuning the r.f. power supply to 1000 volts.

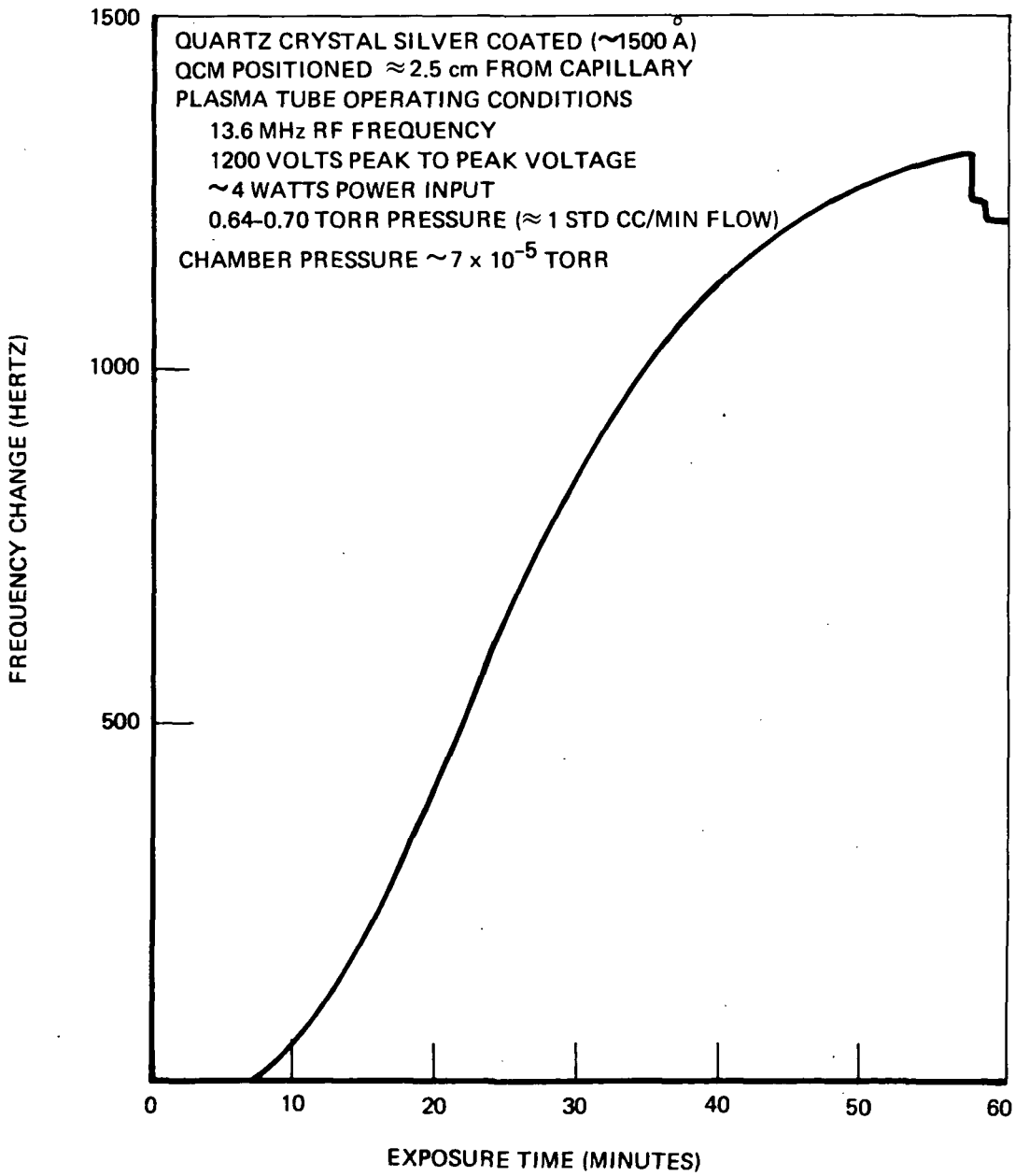

Figure 17 : QCM Response to Oxygen Plasma

frequency change started to occur. These stepwise changes continued to occur (beyond the exposure time shown in Figure 17) until the total frequency change passed through the zero point and beyond. This indicates that there was more material removed from the QCM than had been added. Post test inspection of the crystal showed that the oxidized silver had been flaking off thus explaining the stepwise changes in frequency. The DTM-4 manual gives the following relationship between frequency change and added film thickness.

$$\Delta f \simeq 1/2 \times 10^{8} \rho d \qquad (18)$$

Δf = frequency change (absolute value), Hz

ρ = film density, gm/cm^3

d = added film thickness (absolute value), cm

If terms of added mass per unit area, Δm (gm/cm^2),

$$\Delta f \simeq 5 \times 10^{7} \Delta m \qquad (19)$$

The number of oxygen atoms ΔN added to the silver crystal per cm^2 is given as

$$\Delta N \simeq 0.752 \times 10^{15} \Delta f \qquad (20)$$

The maximum frequency change (just before the stepwise changes started) was 1320 Hz which corresponds to a total atomic oxygen addition of 9.8×10^{17} atoms/cm^2. Assuming that all of these atoms formed silver oxide (AgO)*, all of the oxide remained on the crystal, and that the stepwise changes started when all of the silver was oxidized, the original silver thickness on the quartz crystal was calculated to be 1670 Å. This agrees to within about 10 percent with the manufacturers reported thickness of 1500 Å.

*Post-test x-ray diffraction analysis showed that the oxidized material consisted primarily of AgO with a trace of Ag_2O.

Figure 18 shows the rate of frequency change with exposure time. The rate of frequency change is also shown directly converted, using eqn. (20), to the atomic oxygen flux reacting with the silver. Figure 19 shows the atomic oxygen flux reacting with silver as a function of the total amount of reaction already taken place. As can be seen from these figures, the reaction rate is initially very low, then increases to a maximum and finally decreases as the oxide layer is built up. A possible explanation of this behavior is that initially, with a clean silver surface, the oxygen atoms have a short residence time at the surface and the probability of an oxidation reaction is low. As a thin oxide layer is built up, the residence time is longer (assuming that AgO is permeable to O) and the reaction probability is greatly increased. When the oxide layer becomes thicker yet, the probability for the oxygen atoms to recombine with each other, before they reach the silver surface, increases. These effects would then account for the behavior shown by the data.

The atomic oxygen flux produced by the prototype ACT device should be larger than the maximum flux reacting with the silver. For the conditions of this test, the atomic oxygen flux was thus greater than 0.625×10^{15} atoms/cm^2-sec. Using this information, along with the oxygen flow rate and distance from the capillary, the atomic oxygen concentration in the flow may be determined if the flow pattern is known. If the flow from the capillary is diffuse, then the atomic oxygen concentration in the flow must be greater than 0.0274 atoms per molecule. If the flow is 'line of sight' through the capillary, then the concentration must be greater than 0.002 atoms per molecule.

4.1.4 Plasma Cleaning Experiments

Initially, soot coated samples were used in an attempt to determine the cleaning effectiveness of the ACT prototype device. Tests were made under various conditions of flow rate, power input, run time, and sample distance from the plasma tube capillary. None of these tests resulted in any visible cleaning of the samples. The preliminary cleaning experiments, using the modified original plasma tube at chamber pressures less than

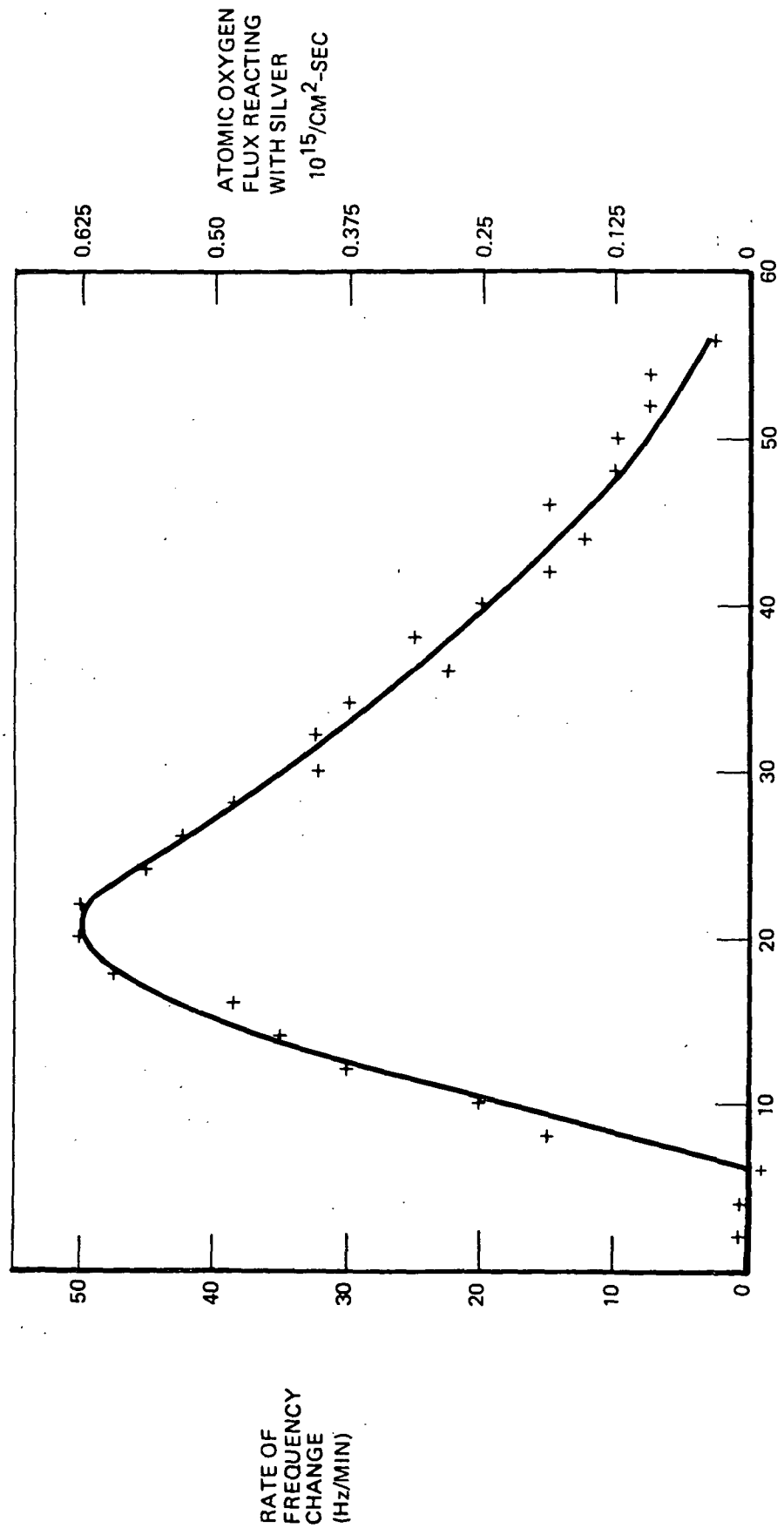

Figure 18 : QCM Response Rate

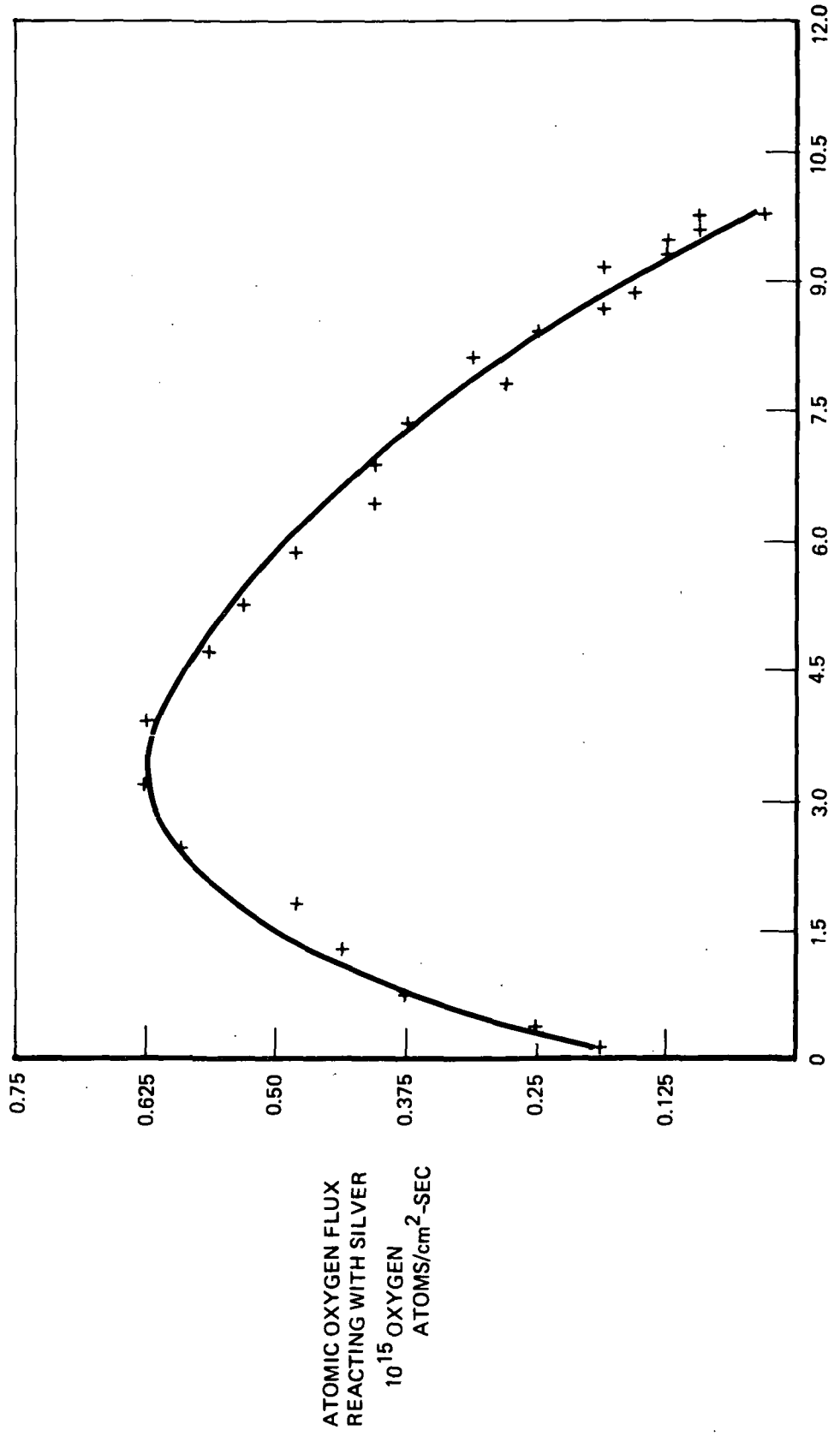

Figure 19 : Rate of Silver Oxide Formation

10^{-4} torr (see Section 3.1), were repeated. It was discovered that the apparent plasma cleaning observed earlier was in reality caused by the high velocity gas stream, impinging on the sample during rapid chamber pumpdown, blowing the soot off the sample.

Since there was no visible cleaning of soot coated samples, more sensitive techniques for detecting carbon removal were than evaluated. The first technique involved overcoating a MgF_2/Al coated mirror with 200-300 Å of vacuum deposited carbon. This carbon coated mirror was first installed about 2.5 cm from the capillary and exposed to the plasma for 1-1/2 hours. The conditions for this test were: an oxygen flow rate of about 1 STD cc/min, r.f. peak-to-peak voltage of 1000 volts and a vacuum chamber pressure of 6×10^{-5} torr. The results of this test showed no visible cleaning of the carbon. The mirror was then moved to within about 1.3 cm of the capillary and the test repeated for an exposure time of 1 hour. Since no cleaning was apparent, the flow rate was increased to 2.5 STD cc/min (vacuum chamber pressure 2×10^{-4} torr) and the test continued for 1-1/2 additional hours. Close visual observation of the mirror after these tests showed no effects of plasma exposure.

Since the plasma cleaning attempts at low flow rates and low chamber pressures had failed, it was decided to reverify the plasma cleaning effect at higher flow rates and chamber pressures where the 'chamber discharge' and 'ignited plume' phenomena occur. The carbon coated mirror was reinstalled, about 1.3 cm from the capillary, and the oxygen flow rate and chamber pressure increased to the point where the 'chamber discharge' occurred. The 'chamber discharge' became apparent when the chamber pressure had increased to about 6×10^{-3} torr with a flow rate on the order of 50 STD cc/min and a peak to peak r.f. voltage of 2000 volts. The chamber discharge appeared to be brightest in the region around the circumference of the plasma tube. In this mode of operation there did not appear to be any visible cleaning, however; by tuning the r.f. power supply, the mode of operation changed to that of the 'ignited plume' and the carbon was rapidly cleaned off the mirror. In the 'ignited plume' mode of operation the capillary appeared to be very bright and

continued to glow red for a short time after the plasma was turned off. This suggests that the discharge was occurring through the capillary as well as in the 'ignited plume'. It should be noted that the r.f. shield tube was not in place during the experiments in which the 'chamber discharge' or 'ignited plume' phenomena occurred. In the event that no plasma tube design changes are made before delivery to NASA, the effect of the r.f. shield on the initiation of the 'chamber discharge' and/or 'ignited plume' phenomena should be evaluated.

Since the possibility still existed that there was some plasma cleaning of carbon at the low flow rates, which could not be detected by visual observation, further tests were made using a carbon coated QCM. An existing quartz crystal, previously coated with 200 Å Al on one side and 200 Å MgF_2 on the other, was over-coated (MgF_2 side) with about 1200 Å of gold. The gold surface was in turn coated with 200 Å of vacuum deposited carbon. The QCM was mounted about 2.5 cm from the capillary. The QCM frequency was monitored under various plasma operating conditions (short of initiating the 'chamber discharge' phenomena) for a total exposure time of about 7 hours. During this time there was no measurable cleaning effect. In fact small frequency changes of the QCM during the tests indicated an increase in the mass, probably caused by gas absorption. These changes were just barely above the background fluctuations in the frequency.

To check the possibility of cleaning contaminant films at the low flow rate and chamber pressure, the carbon coated QCM was contaminated with Butadiene. The crystal was exposed to ultraviolet radiation in an environment of Butadiene at a pressure of 4 torr. The contaminant film thickness buildup on the crystal corresponded to a QCM frequency change of 220 Hz. The QCM was then mounted 2.5 cm from the capillary and exposed to the plasma for 4 hours. The plasma operating conditions were a flow rate of 1 STD cc/min, r.f. peak to peak voltage of 1000 volts and a chamber pressure pf 5×10^{-5} torr. During this exposure there was no measurable indication of plasma cleaning. Assuming that an overall frequency change of 30 Hz could have

been detected above the background instrument instabilities, the cleaning rate, if any, was less than 4×10^{-12} gm/cm^2-sec. After completing the 4 hour exposure the gas flow and chamber pressure were increased to the point where the 'chamber discharge' mode of operation occurred. In this operation mode (flow rate ~50 STD cc/min, chamber pressure 6×10^{-3} torr, r.f. voltage 1800 volts) a measurable cleaning rate of about 2×10^{-9} gm/cm^2-sec was detected. Subsequently the 'chamber discharge' mode spontaneously changed to the 'ignited plume' mode of operation and both the contaminant Butadiene film and the vacuum deposited carbon were rapidly cleaned off the gold surface. The cleaning rate for the 'ignited plume' operation mode was about 10^{-6} gm/cm^2-sec.

A final cleaning experiment using vacuum deposited Fluorescein on a glass plate was conducted. The results of this experiment were the same as those of the other cleaning experiments. No cleaning was observed for low oxygen flow rate and low chamber pressure conditions and rapid cleaning was observed for the 'ignited plume' discharge mode of operation.

4.2 Sputtering Mode Tests

The Gap/Einzel Lens assembly was installed on the prototype ACT device and a Faraday cup assembly was mounted 5 cm downstream of the lens assembly to measure the ion current. The Faraday cup assembly consisted of three shielded cups spaced 1.91 cm apart and each having a 0.476 cm aperature. The center cup was centered along the axis of the lens assembly. The extractor and final accelerator lenses were grounded, and the anode and focusing lenses were each powered by separate high voltage D.C. power supplies. The probe wire (for biasing the plasma) and r.f. electrodes were connected to another high voltage D.C. power supply. An isolation transformer was used to isolate this high voltage from the r.f. power supply. A low voltage D.C. power supply was used for biasing the Faraday cup assembly shield. This bias was set at -100 volts during the tests, however; the degree of bias appeared to have only a slight effect on the

Faraday cup current measurements. The Faraday cup current was measured with an Electrometer (Keithly Model 610R). The on-axis Faraday cup was used for most ion beam current measurements. Off-axis cups indicated an ion beam current about two orders of magnitude less than the on-axis cup.

It was initially thought that the plasma probe wire would have to be biased to a greater positive potential than the anode in order to force ions out through the capillary. However, initial tests of the device showed that the ion current was very small (on the order of 10^{-11} amps) until the plasma probe wire was biased negative with respect to the anode. Figure 20 shows a typical ion current response to the difference in voltage between the probe and the anode. In this case (argon at a pressure of 0.5 torr in the plasma tube) the ion current increases several orders of magnitude as the probe is biased about 500 volts negative with respect to the anode. At this potential difference a D.C. discharge is established between the probe wire and the anode. Once this discharge is established, the r.f. power input seems to have no effect on the ion current. In fact, the r.f. power can be turned off completely without changing the operation of the device.

After the D.C. discharge is established, along with a measureable anode current (greater than about 0.05 ma), the ion current is strongly dependent on the anode current. Figure 21 shows the ion current as a function of the anode current for argon at pressures of 0.25, 0.5 and 1.0 torr. This figure shows that the ion current is a maximum for a pressure of about 0.5 torr. At the lower pressure it takes a larger voltage difference between the probe and anode to establish the D.C. discharge and r.f. power input seems to stabilize the discharge. The data scatter in Figure 21 is primarily due to differences in operating conditions which affect the ion beam current. Figure 22 shows the effect of anode voltage on the ion current for a fixed anode current of 3.0 ma. Data are shown for argon at 0.5 and 1.0 torr and oxygen at 0.5 torr. These data show only a minor effect of accelerating voltage on ion current for voltages above one kilovolt. The data also show that the operation with oxygen is very similar to that with argon.

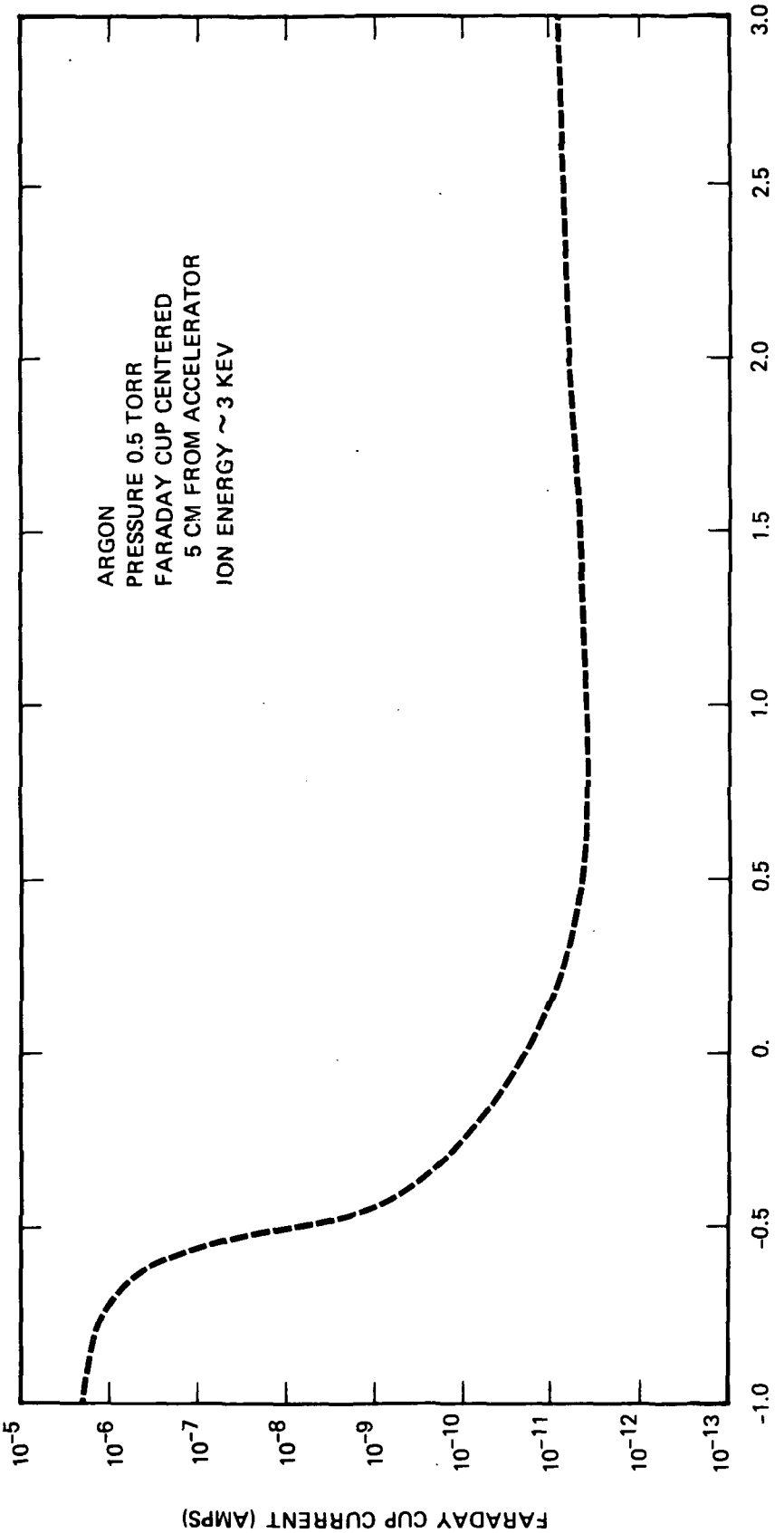

Figure 20 : Typical Ion Current/Probe Voltage Characteristics

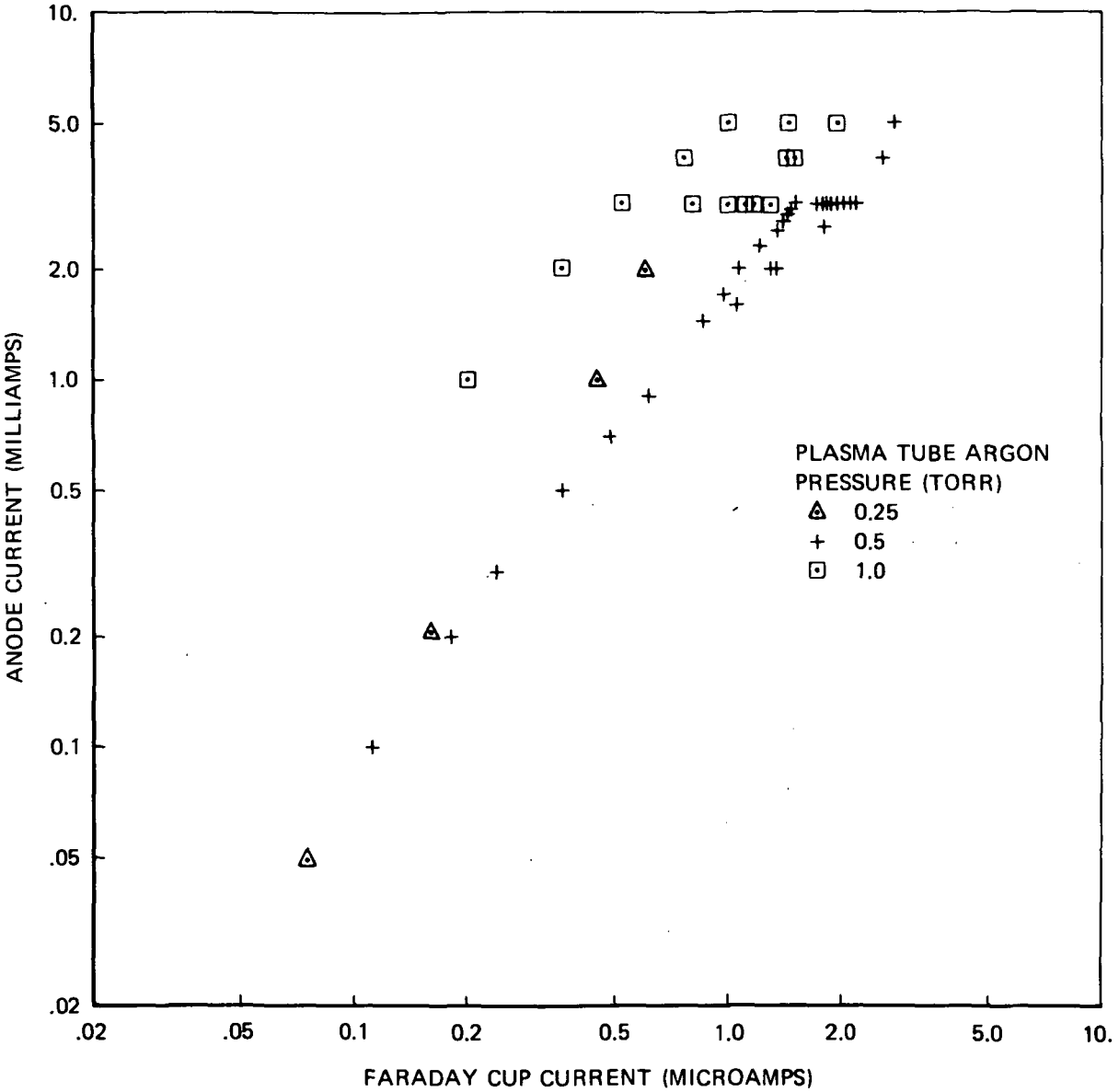

Figure 21 : Ion Current/Anode Current Characteristics

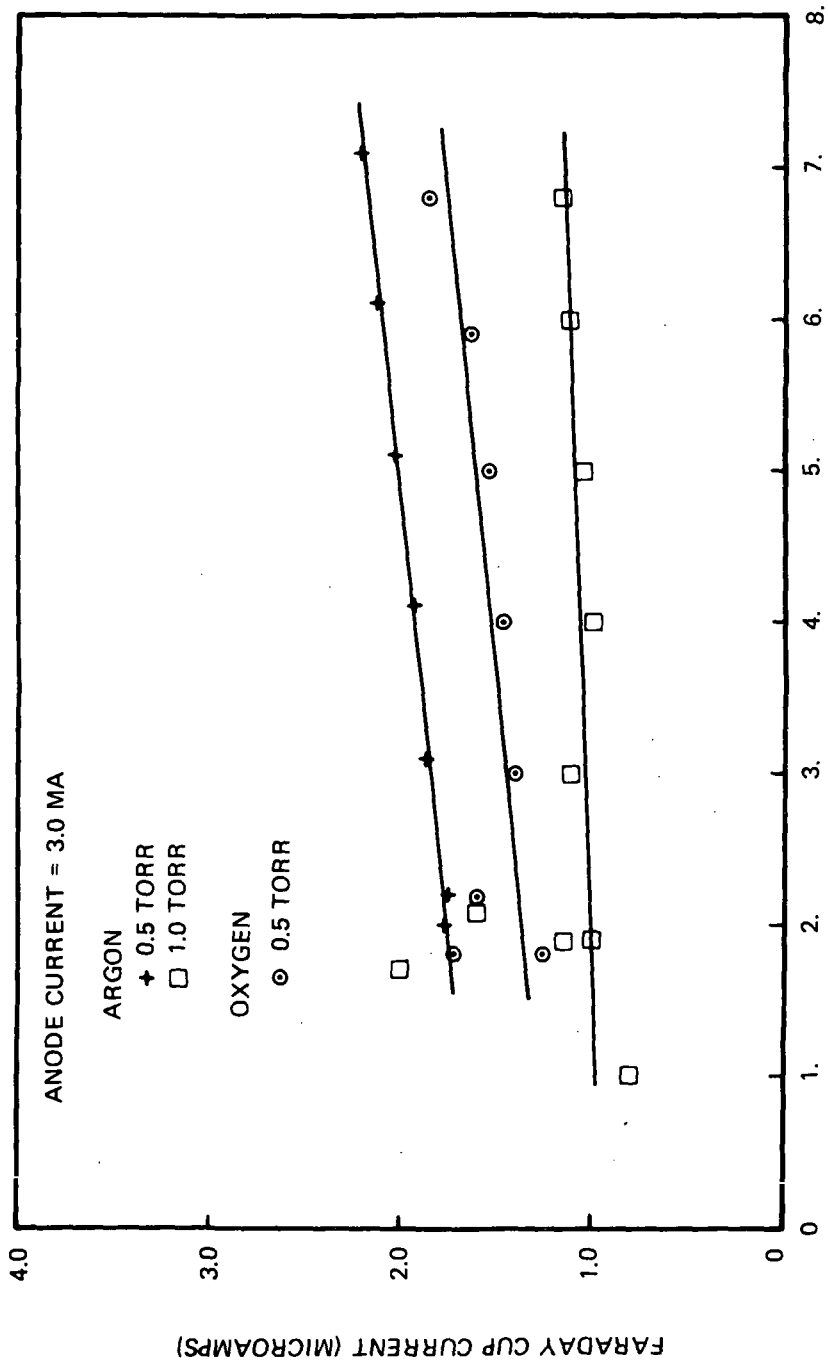

Figure 22 : Ion Current/Anode Voltage Characteristics

Since the sputtering mode tests showed that the operational performance of the prototype ACT device was adequate, a detailed parametric investigation of the operational characteristics was not undertaken. An ion beam current of 1-3 microamps can be obtained without difficulty. This corresponds to an ion flux on the order of 10^{14} ions/cm^2-sec along the centerline, 5 cm downstream of the lens assembly. Post test inspection showed that a circular region (about 1.75 cm dia.) of the Faraday cup shield had been cleaned (a vacuum chamber contaminant film had been deposited during proton irradiation in an earlier program).

5.0 ACT DESIGN

The ACT lab demonstration model design includes both a control console and a plasma generator assembly. A schematic of the control console is shown in Figure 23. As shown in the figure, four functional panels will be included on the console: (1) a gas flow-control panel; (2) a high voltage (5 KV) power supply for operation of electrostatic lenses; (3) an electrostatic-lens voltage-control panel; and (4) an RF power control panel. The flow control panel will feature bulkhead connectors for gas input and output, a foreline vent valve, a dial pressure gauge for monitoring foreline pressure, a Pirani vacuum gauge for monitoring plasma tube pressure, and a plasma-tube ignition indicator. All tubulation for the gas supply system will be 1/4-inch OD (0.635 cm) Teflon tubing, and fittings will be monel. These materials have been selected to allow operation with a corrosive gas in the event that it is required for cleaning silicone contaminants. A schematic of the entire gas supply system is shown in Figure 24. As shown in the schematic, a pressure regulator for a high pressure gas cylinder, will be supplied with the LDM. The portion of the gas supply system in the plasma generator assembly includes; (1) a precision leak valve: (2) a tee fitting (used for connecting the gas supply to the plasma tube, for inserting a high voltage probe into the plasma tube, and for instrumenting pressure with a Pirani guage tube); and (3) the quartz plasma generation tube.

In operation, pressure in the gas supply line upstream of the leak valve (V3), will be maintained at a slightly positive pressure (1-3 psi) using the pressure regulator (R1). In the event that this pressure becomes too high, it can be vented down rapidly with the valve (V2). Pressure in the plasma tube will be controlled by the leak valve (V3). The exact pressure to be maintained in the plasma tube will vary with the desired operating conditions as discussed earlier in the report.

High voltage for electrostatic lenses will be derived from a single power supply and three sets of voltage dividers, as shown in Figure 25. (This

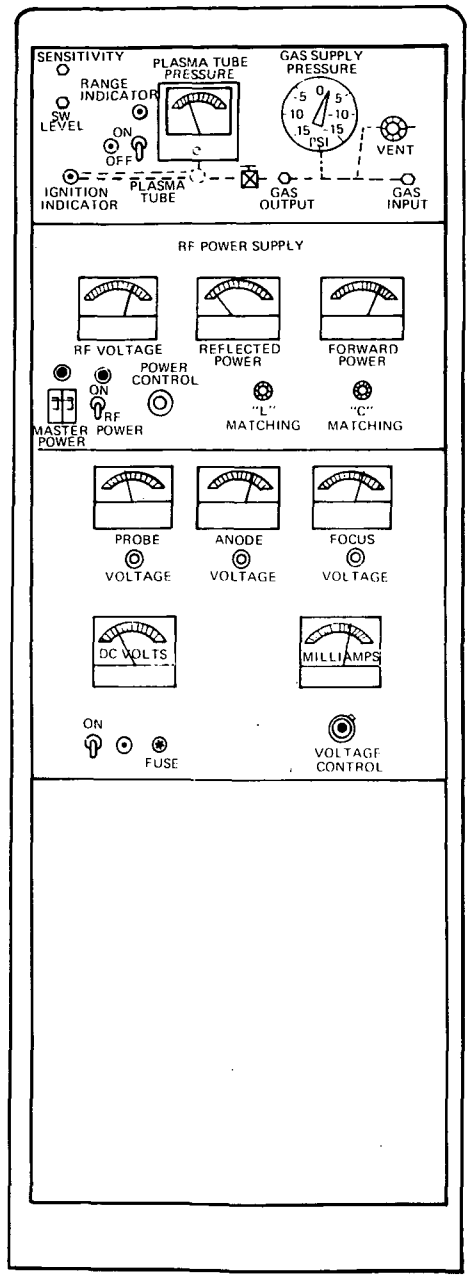

Figure 23 : Schematic of Control Console For Plasma Cleaning Device Lab-Demonstration-Model

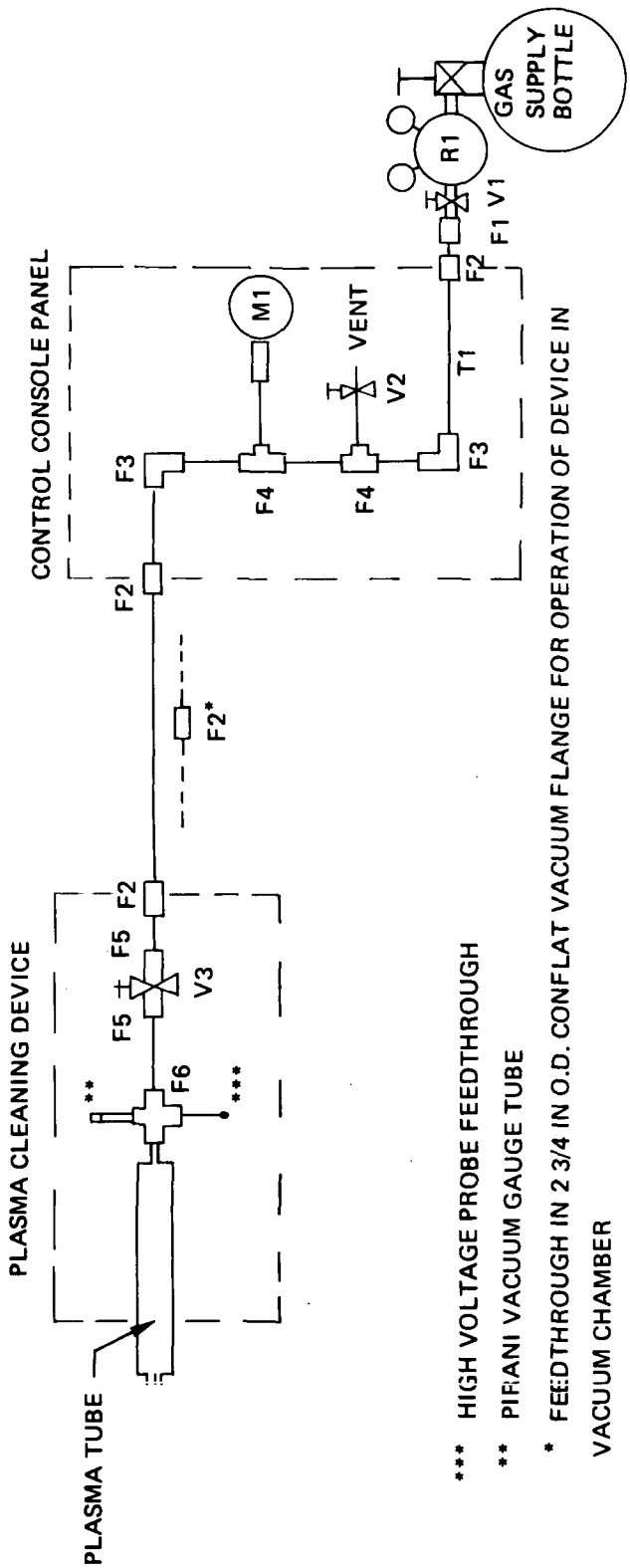

Figure 24 : Schematic of Gas Supply System for Plasma Cleaning Device Lab-Demonstration-Model

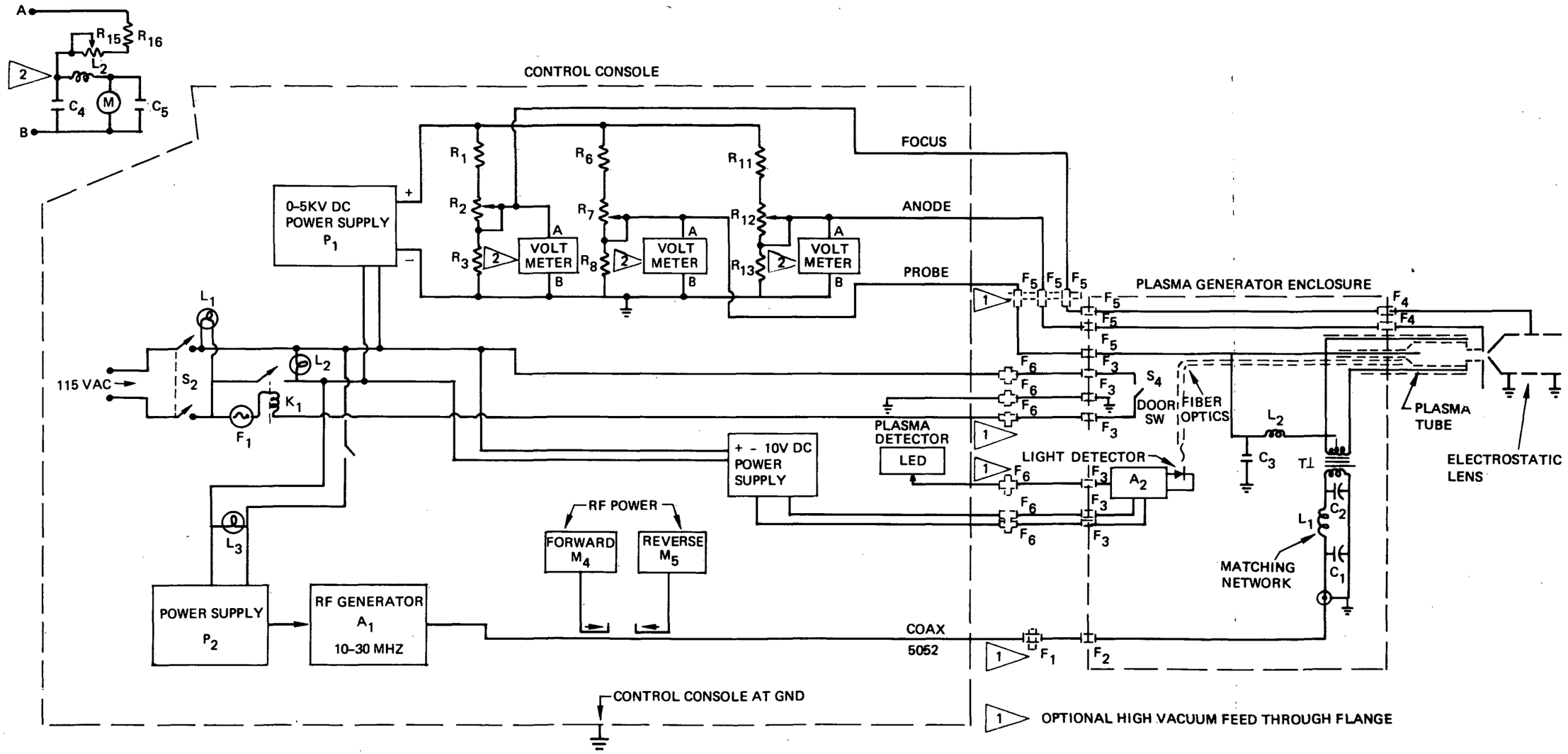

Figure 25 : PLASMA CLEANING DEVICE LAB–DEMONSTRATION MODEL ELECTRICAL DIAGRAM

figure shows an overall electrical diagram for the control console and plasma generator, and includes the wiring schematic for electrostatic lenses.) Each voltage divider will include both fixed and variable resistor. The variable resistor will provide for limited variation in the voltages applied to the focus lens, anode, and plasma probe. Basic voltage control will be established by the power supply.

The r.f. power subsystem will include a variable-frequency power supply (Collins Radio Model 32S-3), which is capable of supplying up to 100 watts continuous-wave power. Frequency of this power supply can be varied from 3 to 30 MHz. The present plasma tube design can be operated satisfactorily at 30 MHz and less than 50 watts of r.f. power. As noted in Figure 25 impedance matching networks will be provided at both ends of the 50 ohm coax transmission cable which transmits power from control console to the plasma generator. It is anticipated that the impedance matching networks can be pre-adjusted before delivery to NASA, and would require no further adjustment for normal operation. A wattmeter will be mounted on the control console panel for monitoring both forward and reflected r.f. power.

During operation of the plasma generator as an ion beam source (for sputtering experiments), the r.f. electrodes can be biased at the probe potential. Commercially available ion sources have traditionally been operated in this manner to maximize the ion current extracted from the plasma exit canal. To allow biasing of r.f. electrodes up to 3 KV, while maintaining the power supply at ground potential, a powdered-core isolation transformer (T1) will be mounted in the plasma generator housing. Voltage isolation of the gas supply line occurs in the Teflon tubing upstream from the leak valve (V3 Figure 24). Breakdown is prevented by supplying gas at relatively high pressure (1 to 3 psi) and by the dielectric strength of the Teflon.

A schematic of the plasma generator assembly is shown in Figure 26. The assembly will consist of a rectangular enclosure of dimensions 7.2 x 11.7 x 11.3 in. (18.3 x 30 x 28.7 cm), which has a plasma generation tube protruding

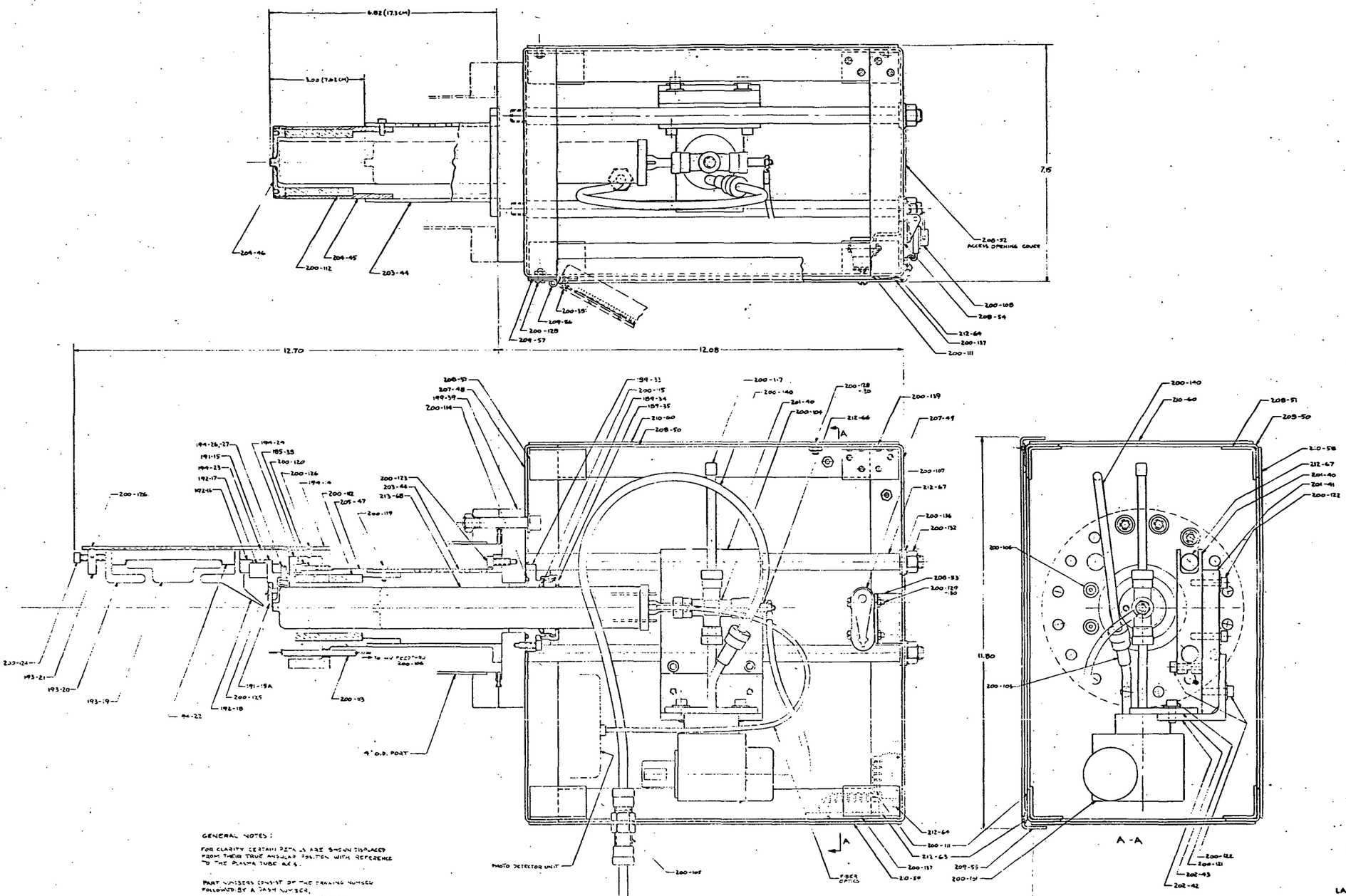

GENERAL NOTES:

FOR CLARITY CERTAIN DETAILS ARE SHOWN DISPLACED FROM THEIR TRUE ANGULAR POSITION WITH REFERENCE TO THE PLASMA TUBE AXIS.

PART NUMBERS CONSIST OF THE DRAWING NUMBER FOLLOWED BY A DASH NUMBER.

EXAMPLE: 189-35 (DASH NO. / DRAWING NO.)

EXCEPT ALL 200-XXX NUMBERS, WHICH ARE STRICTLY IDENTIFYING NUMBERS FOR PURCHASED AND STANDARD PARTS WHICH REQUIRE NO DETAIL DRAWINGS. THESE NUMBERS SHOULD BEAR NO RELATIONSHIP BETWEEN THIS ASSEMBLY DRAWING (SK 5430-200) AND THE SUBASSEMBLY DRAWING.

Figure 26

LAB DEMONSTRATION MODEL
ACTIVE CLEANING TECHNIQUE DEVICE
H.R. 01-05-1973

through a 6-inch O.D. (15.2 cm) vacuum flange on one end of the enclosure. The plasma generator has been designed to allow operation mounted either on a vacuum chamber port, or completely within a vacuum chamber. In the latter case, a mounting bracket would be attached to several tapped holes in the vacuum flange. The plasma generator enclosure serves the dual purpose of r.f. shielding, and facilitating electrical and gas plumbing connections to the plasma tube. The gas supply line and all electrical cables from the control console, connect to bulkhead feedthroughs on the enclosure. To allow mounting of the plasma generator within a vacuum chamber, 2-3/4 inch O.D. (7cm) flanges with matching feedthrough fittings and extra cables, will be furnished with the LDM.

In accordance with the contract requirements, the plasma tube will have a protrusion length with respect to the mounting flange, which can be varied from 9.7 to 17.3 cm. Adjust of the protrusion length will involve loosening of: (1) the "O" ring seal in the 6-inch O.D. (15.2 cm) flange; (2) two clamp screws on the gas inlet assembly; and (3) a locking screw on the telescoping shield tube assembly that surrounds the protruding portion of the plasma tube. The shield tube provides r.f. shielding, retains the plasma tube against atmospheric pressure force, and is a mounting reference for ion source lenses (if used).

6.0 CONCLUSIONS AND RECOMMENDATIONS

Tests of the prototype ACT device in the sputtering mode, showed that a centerline ion flux on the order of 10^{14} ions/cm^2-sec can be produced 5 cm downstream of the lens assembly at a flow rate of about 1 STD cc/min. In the plasma cleaning mode, silver oxidation tests showed a centerline atomic oxygen flux, 2.5 cm from the plasma tube capillary, of more than 0.625×10^{15} atoms/cm^2-sec for an oxygen flow rate of 1 STD cc/min. These test results indicate that the laboratory demonstration model ACT device will be capable of producing a centerline ion flux on the order of 10^{13} ions/cm^2-sec and a centerline atomic oxygen flux greater than 10^{14} atoms/cm^2-sec at the anticipated flow rate of 0.18 STD cc/min.

During prototype testing a serious problem was encountered. Repeated tests showed no measurable contaminant cleaning in the plasma cleaning mode until the chamber pressure and gas flow rate were high enough to produce a 'chamber discharge' phenomenon. Assuming that the species responsible for cleaning are produced in the plasma tube discharge, it must be concluded that not enough of these species survive passage through the capillary to produce measurable cleaning. Assuming that the measured silver oxidation was caused by atomic oxygen (this is consistent with the atomic oxygen attenuation analysis), it must be concluded that the presence of atomic oxygen is not a sufficient condition for cleaning of hydrocarbon contaminants. The silver oxidation might be caused by excited states of molecular oxygen and the atomic oxygen attenuation analysis might be erroneous due to possible contamination on the capillary walls giving a large wall recombination coefficient. However it is more probable that the species responsible for cleaning are either excited oxygen atoms or oxygen ions which are less likely to survive collisions with the capillary wall.

Since the present plasma tube design does not produce the reactive species in sufficient quantity to give measurable contaminant cleaning at low chamber pressures, it is recommended that further studies be made prior to

finalizing the plasma tube design. These studies would be aimed at developing a plasma tube design and operational mode which would provide the appropriate active species at the contaminated surface. Noting that, in the sputtering mode of operation, a D.C. discharge was established through the capillary, a recommended first step would be to determine if the active cleaning species are present downstream of the capillary with a discharge through the capillary.

7.0 REFERENCES

1. Heaney, J. B.: "Results from the ATS-3 Reflectometer Experiment." AIAA Paper No. 69-644 presented at the 4th Thermophysics Conference, San Francisco, California, June 1969.

2. McKeown, D. and W. E. Corbin: "Removal of Surface Contamination by Plasma Sputtering." AIAA Paper No. 71-475 presented at the 6th Thermophysics Conference, Tullahoma, Tenn., April 1971.

3. Cothran, C. A., M. McCargo and S. A. Greenberg: "A Survey of Contamination of Spacecraft Surfaces," AIAA Paper No. 71-475 presented at the 6th Thermophysics Conference, Tullahoma, Tenn., April 1971.

4. Private Communication with Dr. G. Timothy, Harvard College Observatory, Cambridge, Mass., April 1971.

5. Gillette, R. B. and B. A. Kenyon: Applied Optics 10, 3 (1971).

6. Gillette, R. B., W. D. Beverly and G. A. Cruz: "Active Cleaning Technique for Removing Contamination from Optical Surfaces in Space." Annual Report No. 1, Contract NAS8-26385, March 1972.

7. Dushman, S. and Lafferty, J. M., Scientific Foundations of Vacuum Technique, 2nd Edition, John Wiley and Sons, Inc., New York, 1962.

8. Venugopalan, M. and Jones, R. A., Chemistry of Dissociated Water Vapor and Related Systems, John Wiley and Sons, Inc., New York, 1969, page 377.

9. Greaves, J. C. and Linnett, J. W., Trans. Faraday Society, A, pp 1323-1353, (1958).